Received: 14 March 2024 | Revised: 5 May 2025 | Accepted: 2 June 2025

DOI: 10.1002/qj.5040

Quarterly Journal of the Royal Meteorological Society RMetS

RESEARCH ARTICLE

Air–sea interaction in medicanes with atmosphere–ocean–wave coupled regional climate simulations

Fulden Batibeniz[1,2,3] | **Barış Önol**[4] | **Ufuk Utku Turuncoglu**[5] | **Christoph C. Raible**[1,2]

[1]Climate and Environmental Physics, Physics Institute, University of Bern, Bern, Switzerland

[2]Oeschger Centre for Climate Change Research (OCCR), University of Bern, Bern, Switzerland

[3]Institute for Atmospheric and Climate Science, ETH, Zurich, Switzerland

[4]Aeronautics and Astronautics Faculty, Meteorological Engineering, Istanbul Technical University, Istanbul, Turkey

[5]National Center for Atmospheric Research, Boulder, Colorado, USA

Correspondence
Fulden Batibeniz, Climate and Environmental Physics, Physics Institute, University of Bern, Bern, Switzerland.
Email: fulden.batibeniz@unibe.ch

Funding information
National Center for High Performance Computing (UHEM), Turkey, Grant/Award Number: 5004782017; Swiss National Science Foundation (SNF) within the project HARPYIE, Grant/Award Number: IZCOZ0_205416; The Scientific and Technological Research Council of Turkey (TUBITAK), Grant/Award Number: 116Y136; National Center for Atmospheric Research, Grant/Award Number: 1852977; Istanbul Technical University (ITU), Grant/Award Number: 40248

Abstract

Medicanes (Mediterranean hurricanes or cyclones with tropical-like characteristics) have a significant impact on coastal areas and small islands in the Mediterranean region. However, the underlying mechanisms, particularly the role of the air–sea interaction for medicanes, are not fully understood. To investigate these mechanisms, we use the ERA5 reanalysis product as well as four high-resolution simulations conducted with the Regional Earth System Model (RegESM) to study 16 medicane events for the period of 1979–2012 over the Med-CORDEX (Mediterranean-Coordinated Regional Climate Downscaling Experiment) domain. The RegESM model is run in standalone atmosphere, standalone wave, atmosphere–ocean, and atmosphere–ocean–wave settings. Overall, all model settings are able to simulate 15 out of 16 medicane cases compared to the reference ERA5. For most cases, the standalone atmosphere is sufficient to simulate most of the medicane characteristics. However, the analysis shows that the atmosphere–ocean–wave setting improves the storm intensity, while the standalone atmosphere setting tends to show too high wind speeds for the medicanes. For some medicanes, the atmosphere–ocean setting increases the sea surface temperatures, fostering evaporation. This enhanced evaporation contributes to the formation of convective systems by increasing the latent heat flux. Additional wave coupling improves the spatial extent and the timing of the observed medicanes. Due to improved simulation of roughness length over water and its interaction with the atmospheric boundary layer, winds are improved in some cases, leading to a better eyewall at the center of the medicane.

KEYWORDS

air-sea interaction, tropical-like cyclones, extra-tropical weather systems, medicane, mediterranean cyclones, regional climate modeling

1 | INTRODUCTION

Among the numerous cyclones developing over the Mediterranean Sea, there are exceptional storms known as medicanes, which bear a visual resemblance to tropical hurricanes (also called Tropical-like Cyclones – TLCs). These cyclones are influenced by the semi-enclosed nature of the Mediterranean Sea and its complex surrounding topography, which creates favorable conditions for their formation. The Mediterranean Sea also plays a significant role in the complex interactions between Earth system components and the processes that shape the characteristic weather and climate of the Mediterranean basin (Batibeniz *et al.*, 2020). While previous studies suggested that convection plays a crucial role in the occurrence of these low-pressure systems (Cavicchia *et al.*, 2014a), recent research reveals that convection is not necessarily the primary driver of their development (Dafis *et al.*, 2020; Flaounas *et al.*, 2021; Miglietta & Rotunno, 2019). Instead, baroclinic forcing appears to be important (Dafis *et al.*, 2020; Flaounas *et al.*, 2021; Miglietta & Rotunno, 2019). However, the processes leading to the formation of medicanes and the interactions between the atmosphere and the ocean during their occurrence are still not fully understood. Therefore, the purpose of this study is to investigate the mechanisms at the air–sea interface when medicanes exist. We use long-term sensitivity simulations with a high-resolution wave-coupled regional Earth system model, to enhance our understanding of these TLCs and their evolution.

The development and intensity of Mediterranean storms and medicanes are strongly influenced by regional forcing mechanisms, including orographic effects, land–sea interactions, coastal complexity and sea surface conditions. Mediterranean cyclogenesis predominantly occurs near and south of mountain ranges, where synoptic-scale disturbances interact with topography to create lee cyclogenesis and specific cyclone patterns (Flaounas *et al.*, 2022). The Mediterranean's moisture availability, both local and remote, combined with air–sea interactions and sea surface temperatures (SSTs), significantly influences convective intensity and cyclone formation (Bouin & Lebeaupin Brossier, 2020; Flaounas *et al.*, 2019, 2022; Messmer *et al.*, 2017; Miglietta *et al.*, 2011; Pytharoulis, 2018). Strong regional winds (Bora, Mistral-Tramontana, Etesian winds, Sirocco, Libeccio) generate significant wave activity (Lionello *et al.*, 2006), which can lead to storm surges, and changes in sea surface roughness (Lionello *et al.*, 2003). These waves, influenced by atmospheric pressure disturbances, regulate energy exchanges at the air–sea interface (Chen & Curcic, 2016; Hwang, 2016; Janssen, 2008). Therefore, many studies emphasize the importance of air–sea interactions in Mediterranean storm behavior, highlighting the need for accurate modeling of regional forcing mechanisms (Lionello *et al.*, 2006, 2008; Ricchi *et al.*, 2017, 2019; Rizza *et al.*, 2018).

In recent modeling efforts over the Mediterranean basin, air–sea interactions and corresponding wave activity are understood to be drivers. However, few studies have investigated coupled wave interactions with the ocean and atmosphere, and those that exist have focused only on specific cases (Karagiorgos, 2024; Rizza *et al.*, 2021; Varlas *et al.*, 2020). Standalone wave models have been widely used to define extremes over coastal regions, assess flood risks, and better manage and plan coastal activities (Davison *et al.*, 2024; Liberti *et al.*, 2013; Sartini *et al.*, 2015; Thompson *et al.*, 2009). However, these standalone models often underestimate significant wave heights (H_s) (Cavaleri *et al.*, 2020), which could be important for medicanes.

The Mediterranean region has complex topography, characterized by sharp elevation differences along the coastlines and a complex distribution of land and sea. As a result, accurately representing the fine-scale processes that arise from strong surface heterogeneity requires the use of high-resolution modeling in addition to coupled modeling systems (Warner *et al.*, 2008). A recent study has shown that reducing grid spacing from 10 km (parameterized convection) to 2 km (convection-permitting) improves both cyclone track and intensity predictions (Pantillon *et al.*, 2024). The influence of topography, such as the formation of topographic potential vorticity (PV) banners, plays a crucial role in understanding atmospheric dynamics in this region (Flaounas *et al.*, 2022). Additionally, better spatial and temporal distribution of wave activity requires high-resolution wind forcing. Coupled models that account for the interactions between the atmosphere, land, ocean, and waves produce more realistic representations of extreme weather events compared to standalone models (Chen *et al.*, 2013; Katsafados *et al.*, 2016; Zhao & Chen, 2005). Therefore, using a coupled modeling system can provide more accurate and realistic simulations of extreme events in coastal climates.

The detection and monitoring of medicanes, as well as the study of their evolution, is challenging due to the lack of an objective definition. Previous studies have investigated these storms using various methods. These include the use of cyclone detection algorithms to identify storms from satellite images (Nastos *et al.*, 2018; Tous & Romero, 2013), numerical analyses (Arreola *et al.*, 2003; Carrió *et al.*, 2017; Cavicchia *et al.*, 2014a,b; Cavicchia & Von Storch, 2012; Davolio *et al.*, 2009; Fita *et al.*, 2009; Fita & Flaounas, 2018; Homar & Stensrud, 2004; Miglietta *et al.*, 2011, 2015; Moscatello *et al.*, 2008; Mylonas *et al.*, 2019; Picornell *et al.*, 2014; Pytharoulis, 2018;

Reed *et al.*, 2001), meteorological environment studies (Emanuel, 2005; Tous & Romero, 2011), comparisons of standalone and coupled simulation results (Akhtar *et al.*, 2014; Flaounas *et al.*, 2018; Ricchi *et al.*, 2017, 2019; Rizza *et al.*, 2018; Varlas *et al.*, 2020), and the combination of satellite images with modeling approaches (Miglietta *et al.*, 2013). Most of these studies have considered historically recognized events as medicanes based solely on their spiral cloud coverage. A detailed analysis of different medicanes using advanced modeling techniques is still lacking.

In this study, we investigate 16 different medicane events using the first long-term atmosphere–land–ocean–wave coupled simulation for the Med-CORDEX domain. Our aim is to compare medicanes in standalone and coupled model simulations to contribute to a better understanding of the coupling processes of the ocean and waves during medicane development and mature states. To achieve this objective, we conduct four coupled/standalone simulations over the Med-CORDEX region. This approach allows for a quantification of air–sea interactions.

In the following, we present the model and sensitivity simulations (Section 2). We then evaluate the model simulations using climatological mean fields and summarize the results of the sensitivity simulations, focusing on their ability to simulate medicanes (Section 3). Finally, we contextualize the results with existing literature (Section 4) and present our final conclusions (Section 5).

2 | MODEL, SIMULATIONS, DATA AND METHODS

2.1 | Model

We utilize the Regional Earth System Model (RegESM; Turuncoglu, 2019), an Earth system model that can couple four different model components (atmosphere, ocean, wave, and river routing). This allows us to investigate the role of air–sea interaction in simulating key processes for medicane formation. This modeling system is built on the Earth System Modeling Framework (ESMF) library (Theurich *et al.*, 2016) and the National United Operational Prediction Capability (NUOPC) layer, which facilitates connections and information exchange between the model components. The modeling system offers two options for the atmospheric model (Regional Climate Model- RegCM; Giorgi *et al.*, 2012 and Weather Research and Forecasting Model-WRF; Powers *et al.*, 2017; Skamarock *et al.*, 2008), two options for the ocean model (Regional Ocean Modeling System-ROMS; Shchepetkin & McWilliams, 2005; Haidvogel *et al.*, 2008 and Massachusetts Institute of Technology General Circulation Model-MITgcm; Marshall *et al.*, 1997a, b), a wave model (WAM; Monbaliu *et al.*, 2000), and a river routing model (HD; Hagemann & Dümenil, 1997; Hagemann & Gates, 2001). For this study, we used RegCM (4.6.0) as the atmosphere component, ROMS (revision 809) as the ocean component, and WAM Cycle-4 (4.5.3-MPI) as the wave component.

To integrate the atmospheric component into the driver (RegESM-ESMF) and enable data exchange, we modified the Zeng Ocean parameterization provided by RegCM4. The modification allowed the atmospheric model to retrieve information (i.e., SST from the ocean model and roughness length from the wave model to calculate air–sea transfer coefficients and fluxes) from the ocean and wave model components, where atmosphere and ocean/wave model horizontal grids overlapped. To maintain the overall modeling system's stability, it is possible to adjust thresholds for maximum roughness length and friction velocity in RegCM4's configuration file. In this configuration, the atmospheric model sends net surface heat fluxes, net shortwave radiation, surface wind stress components, surface air pressure and net freshwater flux (evaporation-precipitation) to the ocean model and wind field to the wave model. The model coupling time step for data exchange among the model components was set to one hour. For a detailed description of the RegESM, we refer to Turuncoglu and Sannino (2017) and Turuncoglu (2019). Figure 1a provides a schematic representation of RegESM.

2.2 | Simulation setups

The study focuses on the Med-CORDEX domain (Figure 1b) prescribed under the CORDEX framework (Giorgi *et al.*, 2009). Med-CORDEX initiative (Ruti *et al.*, 2016; Somot *et al.*, 2018; www.medcordex.eu) has recently focused on developing fully integrated Regional Climate System Models (RCSMs) for the Mediterranean basin. To contribute to this initiative, we configured the RegESM model for this domain, using both standalone mode (atmosphere-only/wave-only) and coupled mode (atmosphere–ocean−/wave).

We produced standalone and coupled simulations for the period of 1979–2012. The standalone RegCM4 (A12) was forced with ERA-Interim (ERAIN) data using a 12 km horizontal grid spacing and 23 vertical levels. In the coupled simulations, ROMS had a horizontal resolution of approximately 9 km (1/12°; 570×264 grid points) and a vertical resolution of 32 sigma levels ($\theta_s = 5.0$, $\theta_b = 0.4$). The standalone WAM model (W14) was forced by the standalone RegCM4 wind field (A12) with a horizontal resolution of 12 km over the Mediterranean Sea for the

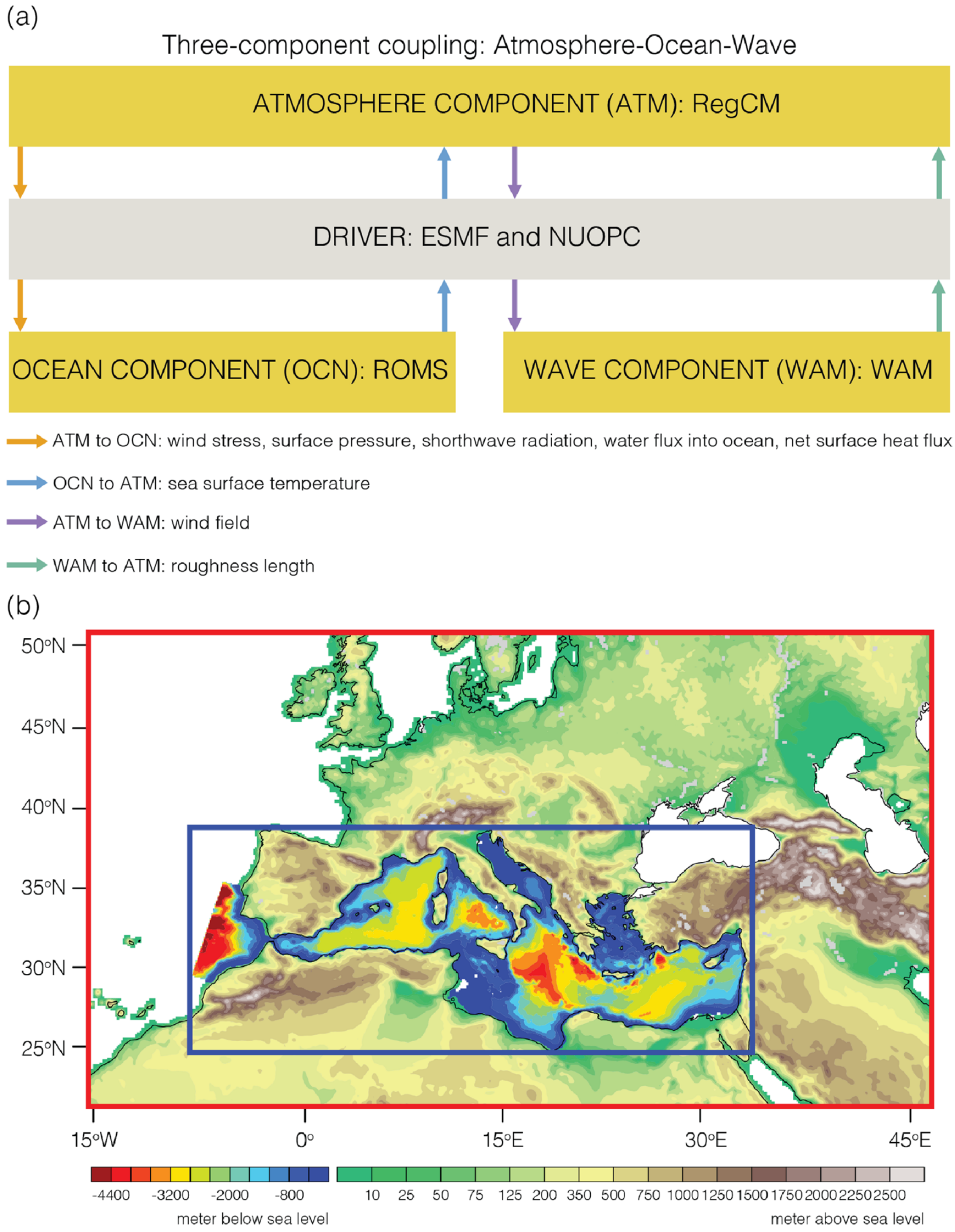

FIGURE 1 (a) Design of the RegESM coupled modeling system. (b) Domain for the RegESM simulations with the topography of the atmospheric model (RegCM4) and bathymetry of the ocean component (ROMS). [Colour figure can be viewed at wileyonlinelibrary.com]

same period. For the W14 simulation, we used a configuration with an approximately 14-km (0.125°) horizontal resolution, 25 frequencies, and 24 directions. A12 used SST provided by the ERSST dataset. In the fully coupled mode of RegESM (AOW), identical standalone configurations of A12 and W14 were used and ROMS was initialized with a combination of World Ocean Atlas 2009 (WOA09; Antonov *et al.*, 2010; Locarnini *et al.*, 2010) and MEDATLAS-II (Fichaut *et al.*, 2003) climatological datasets for January. Additionally, to analyze the effect of wave coupling, we configured RegESM with only atmosphere and ocean components (AO) approximately one month prior to each medicane formation using restart files produced by the AOW setting.

We used a calibrated version of RegCM4 with identical model parameters and configuration as previously validated for 50 km horizontal resolution over the Med-CORDEX region (Turuncoglu & Sannino, 2017). The red line in Figure 1b shows the atmospheric model domain. The A12 configuration includes the Holtslag planetary boundary layer scheme (Holtslag *et al.*, 1990) and Biosphere-Atmosphere Transfer Scheme (BATS: Dickinson *et al.*, 1989) for parameterizing atmosphere–land interaction and boundary layer processes. Additionally, we used the Zeng Ocean parameterization (Zeng *et al.*, 1998) for estimating fluxes over the sea surface and the radiative transfer scheme (Kiehl *et al.*, 1996) for the radiative processes. We employed the cumulus convection scheme of Emanuel (MIT-EMAN; Emanuel, 1991; Emanuel & Živković-Rothman, 1999), Emanuel Sub-Model Parameters (Autoconv. threshold water content ocean: 0.0011; Autoconv. threshold water

TABLE 1 List of simulations.

Run ID	Resolution	ICBC	Active models	Details
W14	0.125° ~ 14 km	A12 wind field	WAM Cycle-4 (4.5.3-MPI)	Standalone
A12	12 km	ERA-Interim, ERSST	RegCM 4.6.0	Standalone
AO	ATM 12 km, OCN 1/12° ~ 9 km	ERA-Interim, ERSST	RegCM 4.6.0, ROMS revision 809/ROMS 3.6	Exchange heat, freshwater fluxes, short wave radiation, surface pressure, SST
AOW	ATM 12 km, OCN 1/12° ~ 9 km, WAM 0.125° ~ 14 km	ERA-Interim, ERSST	RegCM 4.6.0, ROMS revision 809, WAM Cycle-4 (4.5.3-MPI)	Exchange heat, freshwater fluxes, short wave radiation, surface pressure, SST, wind components and roughness length

Abbreviations: AO, ocean components; AOW, atmosphere–ocean–wave; ICBC represents initial conditions and boundary conditions.

content land: 0.005) and the sub-grid explicit moisture scheme (SUBEX; Pal *et al.*, 2000) to represent precipitation (Autoconversion rate for land: 7.50e−04; Autoconversion rate for ocean: 0.500e−03; Raindrop evaporation rate coefficient: 1.00e−03).

As in the atmospheric model, we used the calibrated configuration of ROMS in both AO and AOW simulations (Turuncoglu & Sannino, 2017). Grid spacing is non-uniform and reduces from north to south (Figure 1b; the blue line shows the ocean model domain). Mass exchange from the Strait of Gibraltar is represented by two grid points. The topography of the Mediterranean Sea was created by using the ETOPO1 dataset (Amante & Eakins, 2009) and limiting the minimum depth (*Hc*) to 10 m. Sharp elevation differences in bathymetry for sigma coordinates can create pressure gradient error and disrupt the hydrostatic balance. Therefore, following (Turuncoglu & Sannino, 2017), we used the approach of Sikirić *et al.* (2009) to modify the depths of two contiguous grid points not to exceed 0.25.

The configuration includes the K-profile parameterization (KPP) scheme of Large *et al.* (1994) for vertical mixing, rotated tensors of Laplacian and biharmonic formulation for horizontal mixing. We used the third-order upstream horizontal advection scheme for the momentum equations and tracers (Shchepetkin & McWilliams, 2005) and vertical advection scheme for the fourth-order central scheme along with the parabolic splines reconstruction of vertical derivatives. We defined the background mixing coefficient of tracers and momentum as 1.0×10^{-7} $m^2 \cdot s^{-1}$ and 1.0×10^{-6} $m^2 \cdot s^{-1}$, respectively. For stability, we used constant diffusivity (5.0×10^{11} $m^4 \cdot s^{-1}$) and viscosity (5.5×10^9 $m^4 \cdot s^{-1}$) with the bi-harmonic lateral mixing coefficient. In the momentum equation, we used a quadratic bottom friction of 0.02. We set the time step for the ratio of internal to external mode (barotropic) to 30 s and the time step for the baroclinic internal mode to 120 s.

Precipitation, evaporation, river runoff, and net flow from the Dardanelles Strait (the Black Sea outflow) and Strait of Gibraltar govern the mass balance of the Mediterranean Sea. In our configuration, the discharge of major rivers (Rhone, Po, Ebro, Ceyhan, Adige, and the Tiber) was computed offline using the Max Planck Institute's river routing model (HD). Additionally, river discharge data for the Nile were sourced from the Global Runoff Data Centre (GRDC, Koblenz, Germany) and covers monthly means for the period 1973–1984 to calculate the mean climatological monthly discharge, following the methodology of Turuncoglu and Sannino (2017). This river discharge data were then applied as mass and salinity fluxes in the ocean component.

Currently, there is insufficient information regarding the Black Sea water budget. Therefore, as per Turuncoglu and Sannino (2017), we assumed the Black Sea as a lake and utilized monthly net flow data from Stanev *et al.* (2000), with an annual mean estimated at 8521 $m^3 \cdot s^{-1}$. To maintain volume conservation in the Mediterranean Sea, the total mass flux from the rivers was adjusted by modifying the sea surface height in the Atlantic buffer zone, as detailed by Turuncoglu and Sannino (2017). Furthermore, the net freshwater flux of the Mediterranean Sea, calculated by evaporation-precipitation, was used as a virtual salt flux to the Atlantic buffer zone, also following Turuncoglu and Sannino (2017). Table 1 provides a list of simulations performed in this study and their details. For more information about the parameters and configuration of RegCM4 and ROMS, please refer to Turuncoglu and Sannino (2017).

2.3 | Data and validation

For model evaluation, we investigate the seasonality of key variables such as SST, wind speed and direction, and significant wave height. We compare these variables with the reanalysis data to assess the model's ability to reproduce

climatology. We use one reanalysis and one observation product: the fifth generation of ECMWF atmospheric reanalysis of the global climate with a horizontal resolution of 31 km × 31 km (Hersbach *et al.*, 2020), and the Group for High Resolution Sea Surface Temperature (GHRSST), which provides daily SST data at a resolution of 0.25° × 0.25° for the period from 1982 ongoing (Reynolds *et al.*, 2007). We select ERA5 as our primary reference dataset for all variables and GHRSST specifically for SST validation. ERA5 produces realistic conditions through the assimilation of numerous observational inputs into atmospheric models during its production. It offers the advantage of containing all variables from a single source, preventing inconsistencies and biases that could stem from using multiple data sources. Nevertheless, global reanalyses typically have coarser spatial resolutions that limit their ability to capture the mesoscale dynamics and extreme weather events associated with cyclonic systems. For SST specifically, we also use GHRSST, which combines data from multiple satellite sensors and instruments that undergo continuous quality control and validation. This provides state-of-the-art global SST data with higher spatial resolution, enabling more rigorous validation of our model's SST fields. To allow grid-based comparisons, we linearly interpolate all reanalysis data to the common RCM grid.

2.4 | Medicane analysis

Medicanes are assessed by comparing the standalone atmosphere (A12) and standalone wave (W14) simulations to coupled atmosphere–ocean (AO) and atmosphere–ocean–wave (AOW) simulations to examine the added value of the coupled models in simulating medicanes in the study area. In doing so, we use the case study approach often used for extratropical cyclones (Carrió *et al.*, 2017; Messmer *et al.*, 2017). Based on previous literature and available remote-sensing products (http://meteorologia.uib.eu/medicanes/), we select 16 medicane cases (Table 2). These cases primarily occur in the western and central Mediterranean during the winter and autumn seasons, with a few exceptions.

To analyze the evolution of the medicanes, we apply a simple tracking method to model results and reanalysis datasets. This method estimates the medicane tracks by identifying the sea level pressure minimum for each event in the model outputs and reanalysis data. The identified pressure minima of the analyzed medicanes are then used to define a tetragonal effective area. To account for the movement of medicanes, we add an additional 120 km (10 grid points) to the defined tetragonal area in each direction.

For fair comparison of spatial statistics between the simulations and ERA5, we first identify the centers of cyclones using the minimum mean sea level pressure at their mature state. We then select an equal-sized area around these centers to calculate statistics (e.g., root-mean-squared error RMS, minimum/maximum values, average and average bias; Tables S1–S3). This center-matching approach is necessary since our simulations are not forecasts and do not aim to replicate exact cyclone locations from the forcing data.

To characterize the tropical or extratropical phases of a medicane, we use an adapted version of the phase space diagram employed by Bouin and Lebeaupin Brossier (2020), originally developed by Hart (2003) and modified by Picornell *et al.* (2014) for smaller-scale cyclones. This diagram succinctly describes the cyclone's symmetric characteristics and its core's thermal properties. In this approach, we fit the radius for computing the low-troposphere thickness asymmetry (B) and the thermal winds ($-V_{TL}$ for low troposphere and $-V_{TU}$ for upper troposphere) to the radius of maximum wind at 850 hPa, being approximately 100 km. We define the low troposphere as 925–700 hPa and the upper troposphere as 700–400 hPa as in the modified version. The 100-km radius aligns with several medicane studies (Cavicchia *et al.*, 2014a; Chaboureau *et al.*, 2012; Miglietta *et al.*, 2011; Picornell *et al.*, 2014) and prevents smoothing out the warm-core structure, though it may underestimate the cyclone's extent.

After calculating phase space parameters, we derive two metrics showing the fraction of each medicane's lifetime exhibiting tropical cyclone features (Table 2). The first number represents the portion of a medicane's life that was both symmetric ($B \leq 10$) and had a warm core ($-V_{TL} > 0$). The second number indicates the fraction with a deep warm core ($-V_{TL} > 0$, $-V_{TU} > 0$, and $-V_{TL} > -V_{TU}$). These features are characterized by (1) symmetry, a warm core, and (2) positive values of upper and lower thermal wind, with the lower thermal wind being of greater magnitude.

The cyclone's evolution is visualized using two phase space diagrams: (a) B versus V_{TL} and (b) V_{TU} versus V_{TL}, as illustrated in Figures 7, 9, 11, and 13 below. In the B versus V_{TL} diagram (e.g., Figure 7a), horizontal movement to the left indicates a strengthening cold core or weakening warm core, while vertical movement upward indicates increasing thermal asymmetry. The V_{TU} versus V_{TL} diagram (Figure 7b) shows changes in core strength and depth, with movement toward the lower left corner representing an intensifying cold core or weakening warm core. Green circles mark the beginning of the cyclone's life cycle, and red circles denote the end. Note that these points may not necessarily coincide with the cyclone's formation and decay.

TABLE 2 List of 16 extensively used medicanes.

No	Date	A12	AO	AOW	ERA5	References	Genesis region
M1	19–22 December 1979	0.07, 0.07	0.13, 0.07	0.20, 0.07	0.13, 0.00	(Homar *et al.*, 2002)	W
M2	23–27 January 1982	0.63, 0.11	0.53, 0.11	0.58, 0.00	0.84, 0.74	(Kuo *et al.*, 2002; Pytharoulis *et al.*, 2000)	C
M3	27–30 September 1983	0.67, 0.13	0.60, 0.07	0.60, 0.07	0.53, 0.00	(Rasmussen & Zick, 1987)	C
M4	29–30 December 1984	1.00, 0.71	0.14, 0.00	0.57, 0.14	0.71, 0.00	(Tous & Romero, 2013, 2011)	C
M5	6–9 December 1991	0.13, 0.00	0.13, 0.00	0.00, 0.00	0.67, 0.13	(Tous & Romero, 2013)	C-E
M6	27-29 September 1995	0.27, 0.09	0.36, 0.18	0.36, 0.27	0.27, 0.09	Meteosat data (EUMETSAT)	C
M7	11–13 September 1996	0.18, 0.00	0.27, 0.00	0.36, 0.09	0.55, 0.18	(Cavicchia & Von Storch, 2012; Homar *et al.*, 2003; Tous & Romero, 2013, 2011)	W
M8	3–6 October 1996	0.27, 0.00	0.27, 0.00	0.27, 0.00	0.20, 0.00	(Pytharoulis *et al.*, 2000; Reale & Atlas, 2001)	C
M9	6–11 October 1996	0.17, 0.04	0.39, 0.13	0.35, 0.00	0.09, 0.00	(Fita *et al.*, 2007; Tous & Romero, 2013, 2011)	W-C
M10	7–11 September 2000	0.63, 0.05	0.53, 0.05	0.53, 0.05	0.16, 0.00	(Levizzani *et al.*, 2012; Miglietta *et al.*, 2013)	C
M11	7–10 October 2000	-	-	0.47, 0.07	0.27, 0.00	(Levizzani *et al.*, 2012; Miglietta *et al.*, 2013)	C
M12	10–12 November 2001	0.55, 0.18	0.55, 0.09	0.82, 0.45	0.55, 0.27	(Homar & Stensrud, 2004; Romero, 2008)	W
M13	25–28 May 2003	0.33, 0.00	0.33, 0.00	0.20, 0.00	0.40, 0.27	(Claud *et al.*, 2010; Tous & Romero, 2013, 2011)	W
M14	13–16 December 2005	0.13, 0.00	0.07, 0.00	0.07, 0.00	0.53, 0.20	(Claud *et al.*, 2010; Levizzani *et al.*, 2012)	C-E
M15	31 January–2 February 2006	0.36, 0.09	0.55, 0.00	0.55, 0.27	0.45, 0.18	Meteosat data (EUMETSAT)	C
M16	4–9 November 2011	0.22, 0.00	0.13, 0.00	0.17, 0.00	0.35, 0.13	(Kerkmann & Bachmeier, 2011; Ramis *et al.*, 2013)	W

Note: The genesis regions of these medicines are categorized as West (W), Central (C), and East (E). This figure illustrates two key aspects of medicane lifetimes. The first number in each pair represents the fraction of a medicane's life that was both symmetric ($B \leq 10$) and had a warm core ($-V_{TL} > 0$). The second number shows the fraction with a deep warm core ($-V_{TL} > 0$ and $-V_{TU} > 0$ and $-V_{TL} > -V_{TU}$). Thermal asymmetry (B) ≤ 10 indicates symmetry (non-frontal), while $B > 10$ indicates asymmetry (frontal). For thermal wind ($-V_{TU}$ upper-level, $-V_{TL}$ lower-level), positive values ($-V_T > 0$) indicate a warm core, and negative values ($-V_T < 0$) indicate a cold core.
Abbreviations: AO, ocean components; AOW, atmosphere ocean wave.

3 | RESULTS

3.1 | Model evaluation of simulated variables: SST, wind, significant wave heights

Figure 2a,b present the seasonal comparison between simulated SST and reanalysis datasets (GHRSST, ERA5). We compare simulated seasonal averages of SSTs with the observed climatology for the 1982–2012 period (Figure 2a). The RMS between GHRSST data and the simulations shows similar overall performance (A12: 0.8°C, AOW: 0.88°C) (Figure S1). However, the spatial distribution of biases differs between the models. While the A12 simulation follows ERAIN SST forcing patterns, showing a systematic cold bias across the Mediterranean, the AOW simulation exhibits region-specific biases within ±2°C compared to GHRSST. The warm biases in AOW can be attributed to two main factors: (1) an underestimation of extreme wind speeds over the Gulf of Lion (Figure 3b), particularly Mistral winds, which typically drive cooling in the western Mediterranean through mixing and enhanced

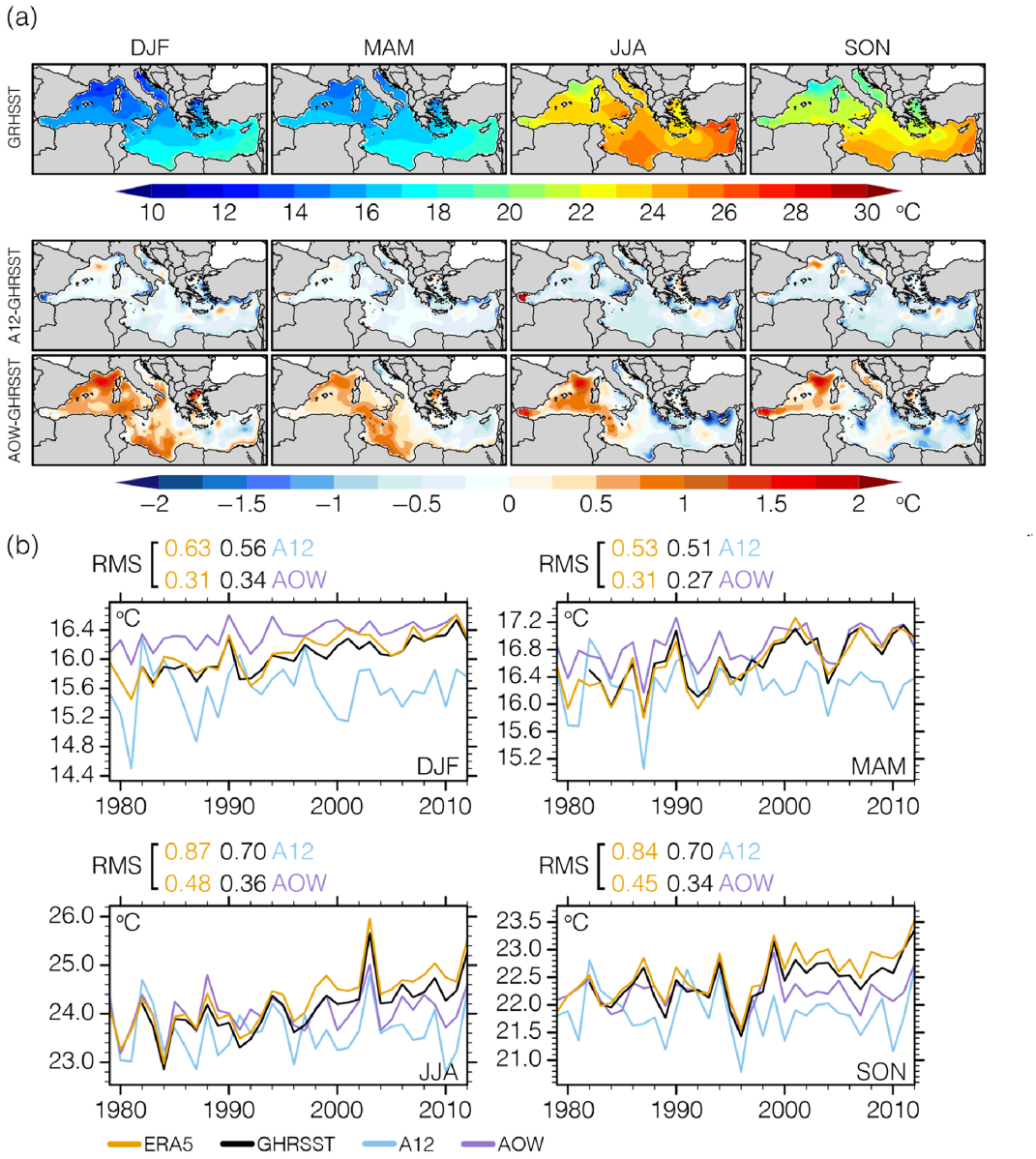

FIGURE 2 (a) Seasonal SST from the GHRSST reanalysis and SST biases from the standalone (A12) and the coupled simulation atmosphere-ocean-wave (AOW) over the Mediterranean Sea for the 1982–2012 period. (b) Inter-annual variability of the domain-averaged seasonal SST over the Mediterranean Sea. The numbers at the top of each panel in (b) represent the root-mean-squared error (RMS) between the simulations and ERA5 and GHRSST reanalysis respectively. [Colour figure can be viewed at wileyonlinelibrary.com]

latent heat loss, and (2) an underestimation of the Po River runoff (~40%–50% lower), which leads to stronger stratification and trapped surface heat due to reduced vertical mixing. The spatial distribution of biases in the AOW simulation (Figure 2a) shows an east–west contrast over the Mediterranean Sea, with warmer SSTs in the western Mediterranean across all seasons and in the central Mediterranean during winter and spring, while SSTs are cooler in the eastern Mediterranean compared to GHRSST. The AOW improves the representation of SSTs, especially over the southern coastlines of the Anatolian Peninsula in winter, spring, and fall, as well as the western coastlines of Italy in summer and autumn compared to A12.

The analysis of inter-annual SST variability (Figure 2b) shows that the domain-averaged seasonal SSTs vary in the range of ±1.5°C across all datasets and seasons. The A12 simulation (ERAIN dataset) consistently underestimates SSTs in almost all seasons compared to GHRSST and the ERA5 dataset, particularly toward the end of the simulation period. The AOW simulation resembles the SST variability of GHRSST and ERA5 datasets and shows lower RMS values than the A12 simulation in

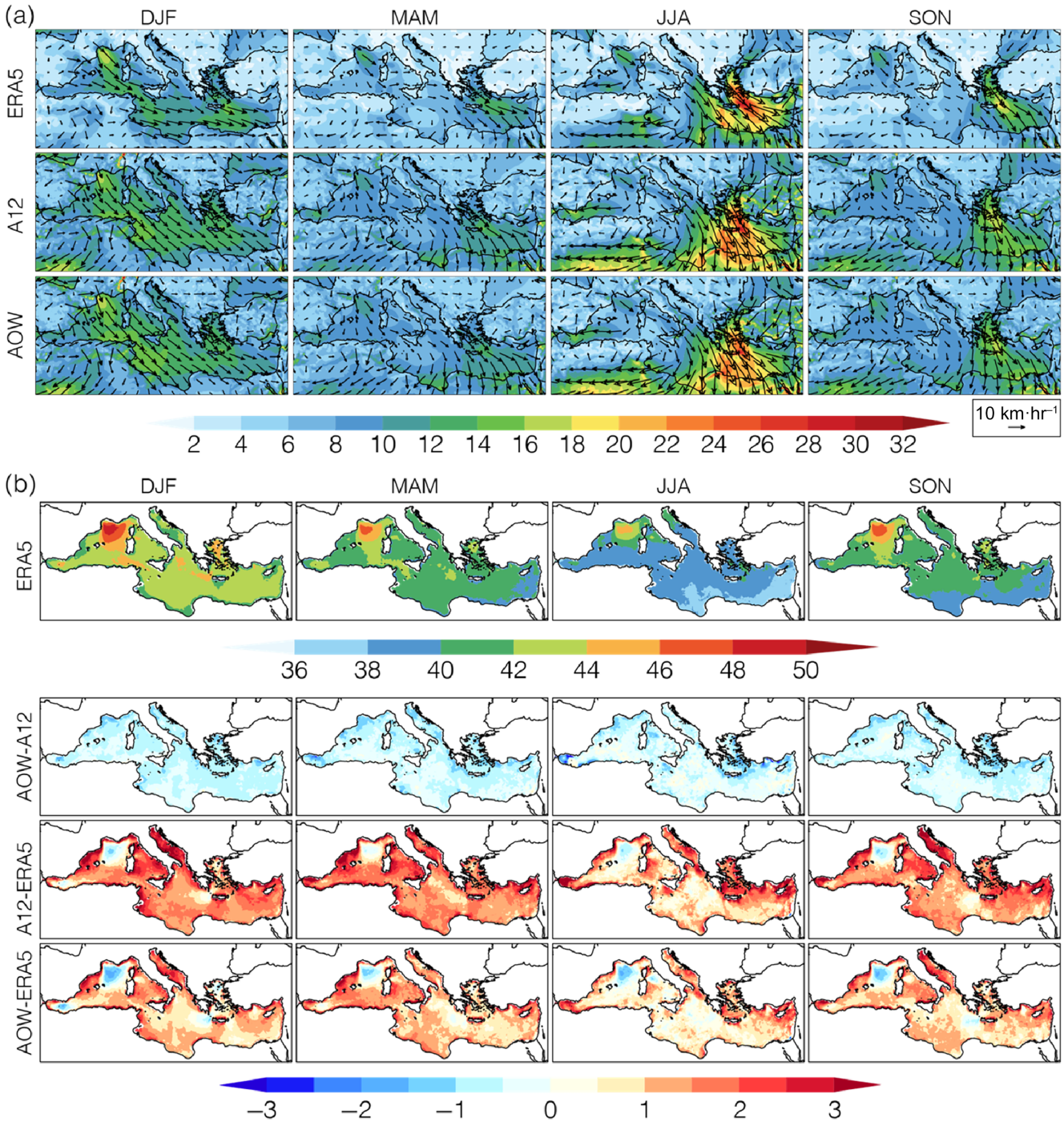

FIGURE 3 (a) Seasonal near surface (at 10 m) wind speed and direction climatology and (b) strong seasonal wind speed (above 36 km·hr^{-1}) of ERA5 and differences between atmosphere-ocean-wave (AOW) and A12, the standalone and the coupled simulation for the 1979–2012 period. The wind vectors in (a) are rotated to earth coordinates for the model simulations, and the unit vector is set to 10 km·hr^{-1}. [Colour figure can be viewed at wileyonlinelibrary.com]

all seasons, particularly in winter and spring (0.31°C against ERA5 and 0.27–0.34°C against GHRSST). A warming trend observed in GHRSST and ERA5 from the mid-1990s, which has also been reported in previous studies (Nykjaer, 2009; Pastor *et al.*, 2020; Skliris *et al.*, 2012), is partially captured by AOW, especially in winter and spring, though it underestimates the warming after 2000 in summer and autumn. Overall, AOW provides more realistic representation of the interannual variability of SST.

In Figure 3a, we compare the simulated (A12 and AOW) near-surface (at 10 m) wind speed and directions with the ERA5 reanalysis dataset for the period 1979–2012.

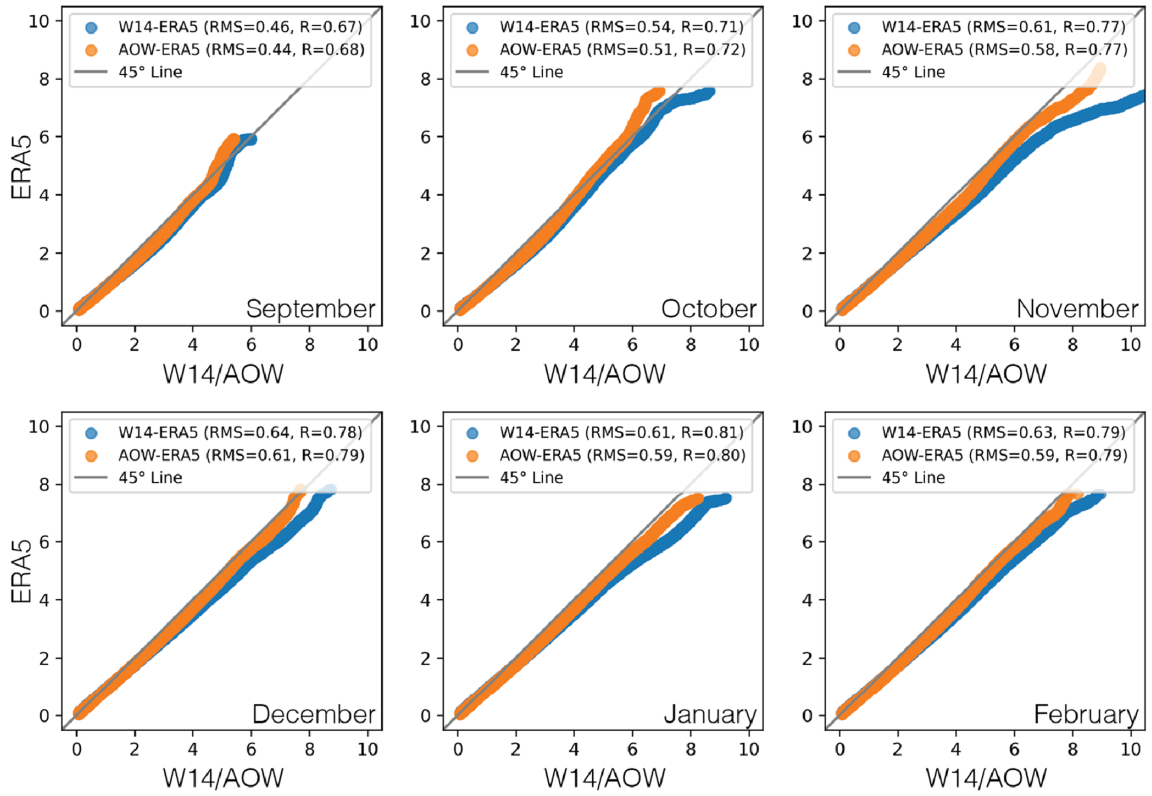

FIGURE 4 Quantile–Quantile (Q–Q) plots comparing significant wave heights from ERA5 reanalysis with model simulations (standalone and coupled) for the Mediterranean Sea during autumn and winter months (1979–2012). Atmosphere-ocean-wave (AOW) and Wave (W12) are compared against ERA5. Root-mean-squared error (RMS) values and correlations between model simulations and ERA5 (calculated before Q–Q plot sorting) appear at the top of each panel. Diagonal lines represent the 45° reference line indicating perfect agreement. [Colour figure can be viewed at wileyonlinelibrary.com]

Both simulations show good agreement with ERA5 reanalysis dataset across all seasons. The AOW and A12 simulations slightly overestimate wind speeds compared to ERA5, except over the Gulf of Lion and southern Anatolian Peninsula. The AOW simulation produces higher wind speeds (closer to ERA5) than A12 over the Gulf of Lion throughout all seasons, indicating AOW improves wind representation in this region. However, along Tunisia's coastline in winter, the AOW simulation produces higher wind speeds than A12, showing a stronger positive bias compared to ERA5. In spring, summer and fall, the AOW simulates lower wind speeds than A12 over the Aegean Sea, resulting in a negative bias compared to ERA5.

For the evaluation of extreme winds, we analyze the average extreme seasonal wind speeds above 36 $km \cdot hr^{-1}$ over the Mediterranean Sea in Figure 3b. In the coupled model, the atmospheric model provides surface conditions (such as wind speed, friction velocity, and wind direction) to the wave model and receives surface roughness to calculate air–sea transfer coefficients and fluxes. When the wave-induced surface roughness in AOW exceeds that of the A12 model, this interaction leads to reduced wind speeds and enables the coupled model to better represent extreme wind fields. Compared to A12, the AOW simulation better represents extreme wind speeds throughout the Mediterranean Sea in all seasons, with the exception of the Gulf of Lion region.

To evaluate the wave model's sensitivity to different wind forcings, we compare ERA5 against two simulations: W14 (forced by the A12 wind field), and AOW (with coupled wind field). Figure 4 shows Q–-Q plots of significant wave height (H_s) comparing both simulations against ERA5 reanalysis data over the Mediterranean Sea during winter and autumn months. Under calm weather conditions in autumn and winter (H_s less than 3 m), the W14 and AOW simulations perform similarly. However, discrepancies between the two simulations begin to emerge for H_s above 4–5 m, with the W14 simulation producing higher H_s values under extreme conditions. ERA5 and AOW exhibit very similar distributions in both seasons. According to Wiese *et al.* (2018), WAM model simulations forced with ERA5 winds have improved accuracy (smaller positive bias) compared to those using ERAIN data, which can be attributed to ERA5's higher spatial resolution. Our results support these findings, as W14 overestimates higher H_ss. This confirms that the AOW simulation

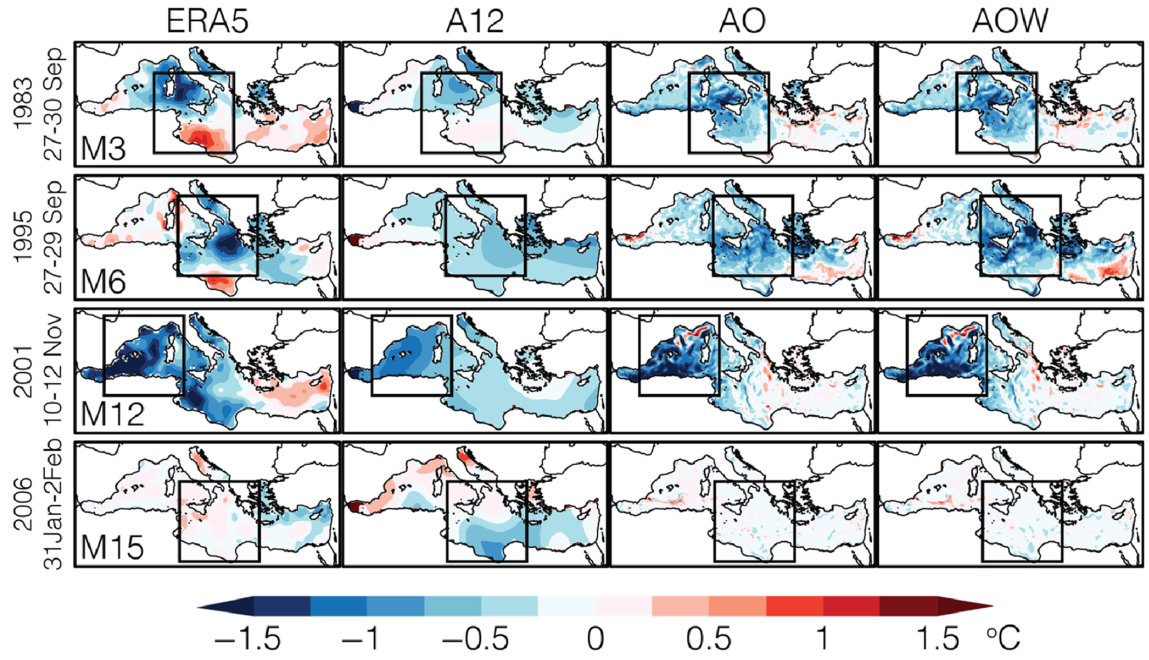

FIGURE 5 Sea surface temperatures (SST) anomalies of the selected four medicanes at their approximate mature stage location (shown by black squares). The anomalies are calculated by substracting SST values from two days before the mature stage from those observed two days later, highlighting short-term temperature changes as medicanes pass through. [Colour figure can be viewed at wileyonlinelibrary.com]

provides the best performance in representing H_s. The reduction in the H_s can be attributed to reduced extreme wind speeds resulting from the WAM model's roughness length input to the coupled model. While there are no significant differences in calculated RMS and correlation values (calculated before Quantile–Quantile [Q–Q] plot sorting) for H_ss across models, the improvement becomes evident when examining higher H_s values.

3.2 | Air–sea interaction of medicanes during their mature state

To evaluate the performance of the different simulations, we analyze 16 events (Table 2). Most simulations accurately represent 15 of the 16 medicanes with M11 being absent in A12 and AO simulations. According to the metric of the warm-core structure and thermal symmetry (Section 2.4, Table 2), we find that 13 out of 16 medicanes in ERA5 exhibit these tropical features for at least 20% of their life cycle. The model simulations show comparable results for at least 20% of their life cycle: AOW represents 13 cases, while AO and A12 represent 10 cases each. This shows that the AOW simulation better reproduces the symmetrical and warm-core features of medicanes. For the second metric (Section 2.4), all simulations align with ERA5, indicating that only few of the selected cases show a deep warm-core structure throughout their life cycle. Overall, the A12, AO, and AOW simulations perform similarly for 11 events, with slight variations. Notably, the wave component influences the outcomes in M3, M6, M12, and M15 events. To understand where models differ from each other, we focus on these four cases, presenting their SST anomalies (Figures 5 and S3) and key parameters for spatial and temporal analysis (Figures 6–14) and statistics (Tables S1–S3). Detailed statistics are available in the Supporting Information, though not all table information is discussed here. The remaining cases are briefly discussed, and related figures are provided in the Supporting Information (Figures S4–S7).

Starting with the M3 event (27–30 September 1983), the AOW simulation accurately represents the strong convergence of moisture flux associated with the cyclonic winds (Figure 6). This convergence toward the cyclone's center, combined with higher latent heat flux values (Table S2), contributes to the development of the convective system in the coupled simulations. Figure 7a shows a strengthening of the warm core structure across all models and reanalysis. Compared to ERA5, the initial cyclone tracks in the A12, AO, and AOW simulations exhibit similar locations but shift southwestward. This shift is more pronounced in the coupled simulations, causing the cyclones to encounter a continental barrier and change their direction towards the southeast. The southwestward movement and warmer SSTs (Figure S2) result in higher latent heat flux values in the AOW (up to ~442 $W \cdot m^{-2}$) compared to ERA5 (up to ~305 $W \cdot m^{-2}$) and A12 (up to ~347 $W \cdot m^{-2}$). The AOW simulation shows a positive

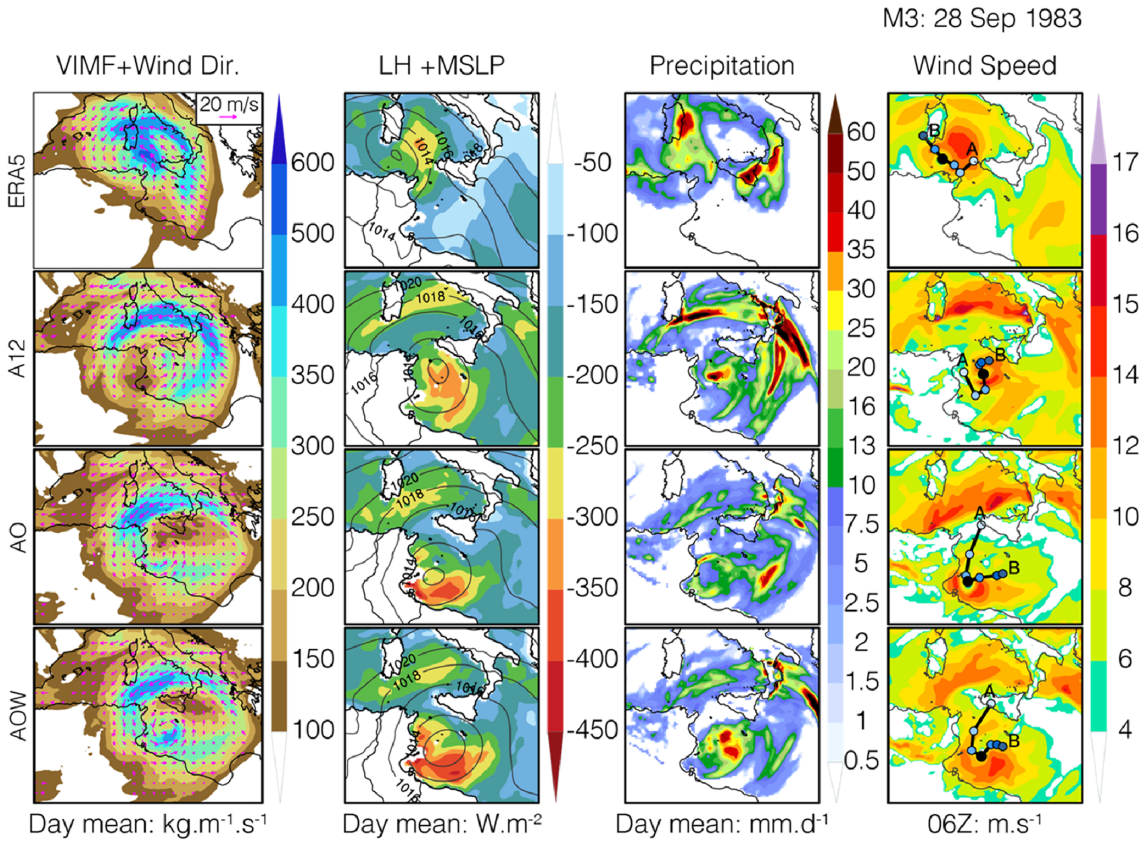

FIGURE 6 Day mean of vertically integrated moisture flux ($kg \cdot ms^{-1}$) and wind direction (first column), day mean of latent heat flux and mean sea level pressure ($W \cdot m^{-2}$, hPa) (second column), day mean of precipitation ($mm \cdot day^{-1}$) (third column), and wind speed at the approximate mature stage of the 27–30 September 1983 medicane (fourth column). Circles in the fourth column shows the medicane's movement; A marks 18 hours before the mature stage, the filled circle indicates the mature stage, and B marks 18 hours after the mature stage. [Colour figure can be viewed at wileyonlinelibrary.com]

average wind speed bias ($+0.72\ m \cdot s^{-1}$), though the maximum wind speeds in the coupled models (AO: $14.88\ m \cdot s^{-1}$, AOW: $14.83\ m \cdot s^{-1}$) are closer to ERA5 ($14.92\ m \cdot s^{-1}$) than A12 ($15.6\ m \cdot s^{-1}$). This explains why the cyclone in AOW is deeper (1010.29 hPa) and more closely matches ERA5 (1009.83 hPa) than in the AO (1011.74 hPa) and A12 (1011.48 hPa) simulations. Still, the spatial RMS is the least for the MSLP in A12 simulation, and lower in wind speed in the coupled simulations (Table S1). Unlike the coupled simulations and ERA5 (and GHRSST), A12 fails to reproduce the magnitude of the SST cooling two days after the mature stage compared to two days before the mature stage (Figures 5 and S3). The cyclone's classification is complex due to frontal structures in the precipitation. This is also visible in the phase space diagram where the cyclone transitions from a cold to a warm core, with a symmetric, shallow warm-core structure developing between 925 and 700 hPa (Figure 7a). The cyclone does not develop a deep warm-core structure typical of tropical cyclones, which is reflected in the low temperatures between 700 and 400 hPa (Figure 7b). While all models reproduce these aspects, they differ in the location and magnitude of peak precipitation (ERA5: 53.05, A12: 73.63, AO: 37.54, AOW: 50.64 [in $mm \cdot day^{-1}$]) and average daily precipitation values above $1\ mm \cdot day^{-1}$ (ERA5: 10.81, A12: 10, AO: 8.48, AOW: 11.71 [in $mm \cdot day^{-1}$]).

Another fall-season medicane (M6: 27–29 September 1995), located in the Ionian Sea, shows that the storm's location is better replicated with the AOW simulation compared to the A12 and AO simulations (Figure 8). The cyclone and associated moisture flux shift eastward in the AO simulation and even further over land in the A12 simulation. Additionally, the AOW simulation more accurately represents the pressure gradient and latent heat flux (up to $\sim 337\ W \cdot m^{-2}$; ERA5 shows up to $\sim 365\ W \cdot m^{-2}$) as a source of energy, especially over the Gulf of Gabes, compared to the A12 (up to $\sim 253\ W \cdot m^{-2}$) and AO (up to $\sim 288\ W \cdot m^{-2}$) simulations. Both AO and AOW simulations produce higher SST values (~26°C) than A12 simulation (~25°C). These higher SST values increase evaporation and fuel the storm with an increased latent heat flux, whereas A12 underestimates latent heat fluxes (Table S2).

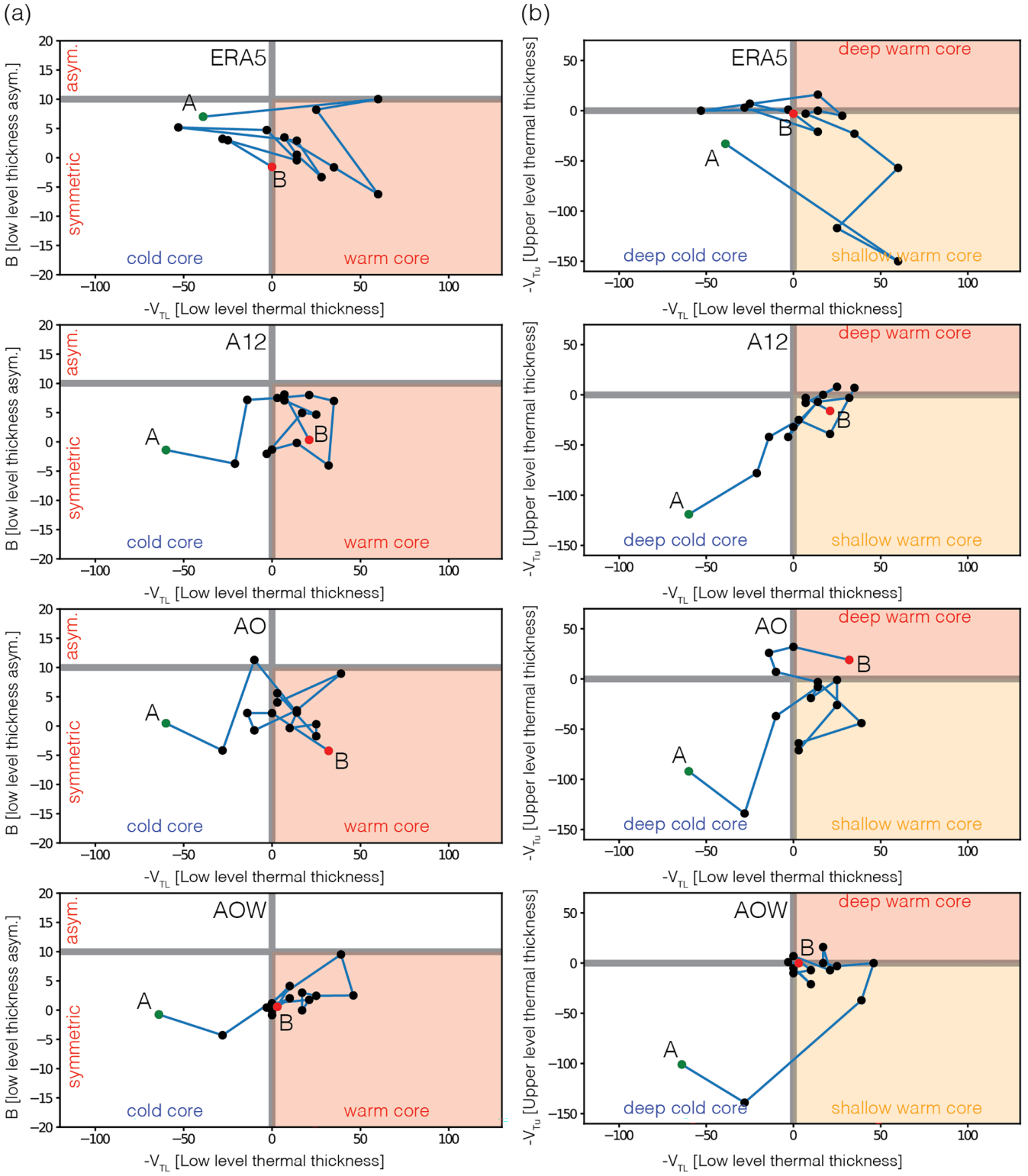

FIGURE 7 Phase diagram of the 27–30 September 1983 medicane for ERA5, A12, ocean components (AO), and atmosphere-ocean-wave (AOW) simulations. The phase evolution of (a) B vs. $-V_{TL}$ and (b) $-V_{TU}$ versus $-V_{TL}$ is shown at six-hour intervals. A indicates the beginning and B indicates the end of the medicane's life cycle. [Colour figure can be viewed at wileyonlinelibrary.com]

Although both AO and AOW simulate the SST cooling two days after the mature phase, the magnitude is stronger in AOW resembling ERA5 and GHRSST (Figures 5 and S3), which explains the higher LH values in AOW. The location and direction of this storm help explain the performance differences between models. In the A12 simulation,

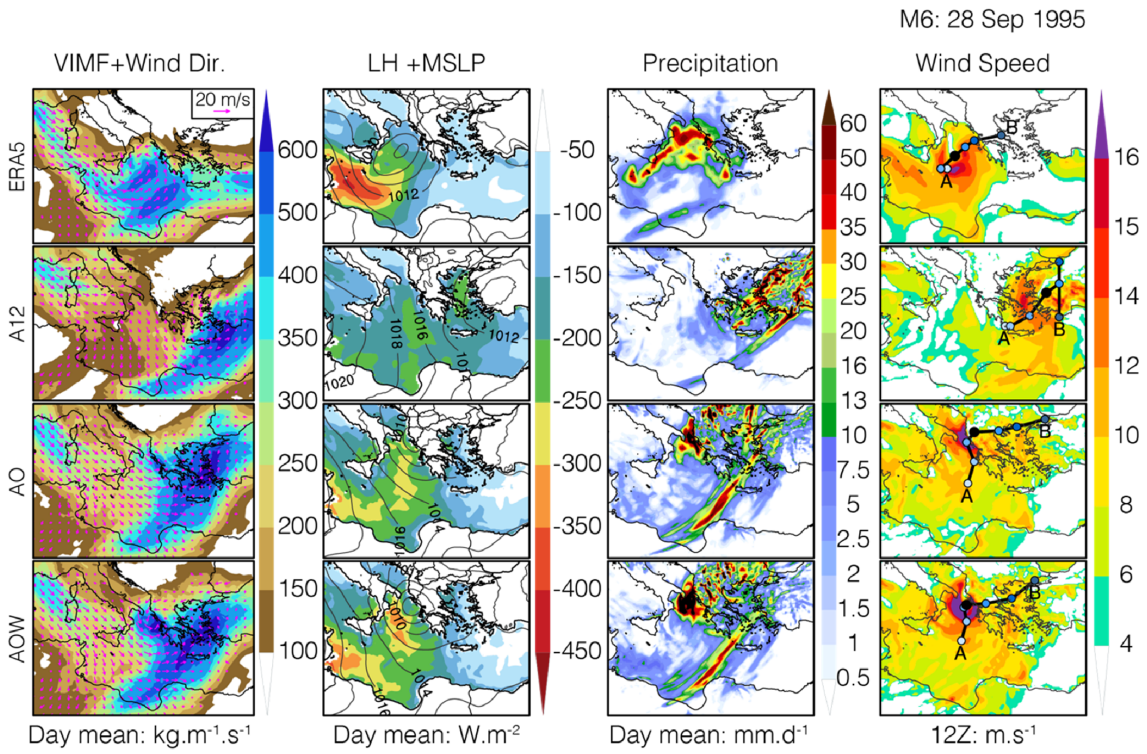

FIGURE 8 Same as in Figure 8, but for the 27–29 September 1995 medicane. [Colour figure can be viewed at wileyonlinelibrary.com]

wind speeds are higher over the Aegean Sea instead of the Adriatic Sea, the pressure gradient is ~3 hPa higher than in ERA5, and the medicane travels eastward towards the Anatolian peninsula. In contrast, both AO and AOW simulations show the medicane moving towards the Adriatic Sea, consistent with ERA5. While both coupled models perform similarly, the wave-enabled version (AOW) produces a deeper system with higher latent heat flux and maximum wind values, leading to stronger cyclone intensification and increased energy gain from the sea surface. This is also visible in phase space diagrams, where the AO and AOW simulations developed a deep warm core similar to ERA5, with AOW maintaining it longer than both ERA5 and AO, while A12 never developed a warm core (Figure 9). As a consequence, AOW strongly overestimates the maximum of precipitation (262.9 mm·day^{-1}) compared to ERA5 (59.6 mm·day^{-1}) (Table S2).

Figure 10 (M12: 10–12 November 2001) show an intense medicane event with extremely high winds and strong gradient zones. All three simulations exhibit similar convergence of moisture in space. The spatial distribution of moisture is also quite similar across the simulations and reanalysis. Overall, all simulations represent the cyclone well compared to ERA5, though with some notable differences: Wind speeds during the mature stage vary, with AOW (27.91 m·s^{-1}) best resembling ERA5 (24.83 m·s^{-1}), compared to A12 (34.25 m·s^{-1}) and AO (31.93 m·s^{-1}). The AOW simulation also captures a more distinct eye formation in the precipitation field over southwest Sardinia. While average precipitation is very similar, maximum precipitation values differ across simulations (A12: 225.27 mm·day^{-1}, AO: 176.49 mm·day^{-1}, AOW: 205.65 mm·day^{-1}) and are notably higher than ERA5 (97.19 mm·day^{-1}), indicating overestimation of maximum precipitation across all simulations. Spatial accuracy analysis through RMS errors shows AOW performing best in wind speed representation (8.74 m·s^{-1} compared to A12's 9.55 m·s^{-1} and AO's 10.01 m·s^{-1}), though showing higher MSLP errors compared to the other simulations (Table S1). The coupled simulations (AO and AOW) produce more realistic SSTs, showing 2–3°C higher values at the medicane's center compared to A12, matching ERA5 data (Figure S2). The SST cooling two days after the mature phase in both AO and AOW simulations closely aligns with ERA5 and GHRSST (Figures 5 and S3). Phase space diagrams show that all cyclones in the model simulations transition from shallow warm core to deep warm core as in ERA5 (Figure 11). While all simulations show lower pressure values than ERA5 and higher wind speeds, the AOW simulation develops the strongest deep warm core structure, explaining its more pronounced eye formation and SST cooling. The varying latent heat flux values across simulations (ranging from 603 to 624 W·m^{-2}) contribute to differences in cyclone intensity and structure.

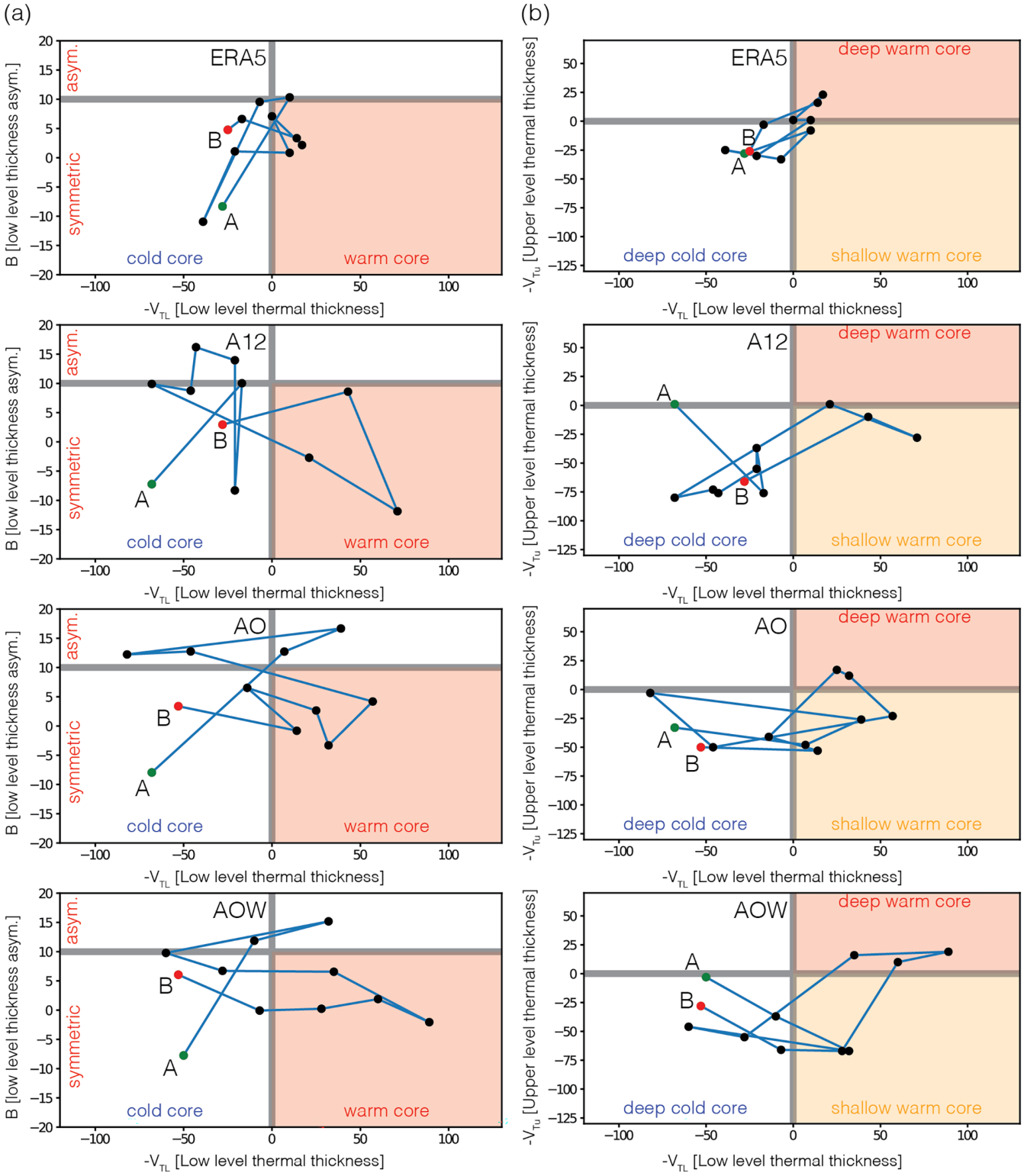

FIGURE 9 Same as in Figure 9, but for the 27–29 September 1995 medicane. [Colour figure can be viewed at wileyonlinelibrary.com]

For medicane M15 (31 January–2 February 2006), the AOW simulation shows better performance in several key metrics compared to other simulations (Figure 12, Tables S1–S3). Its vertically integrated moisture flux distribution aligns closely with ERA5 data, and its minimum MSLP (~997 hPa) nearly matches the core pressure of ERA5 (~995 hPa), while A12 and AO both overestimate the pressure (~1002 hPa). AOW's steeper MSLP gradient results in the lowest spatial RMS error (2.01 hPa, Table S1) among the models. The AOW simulation

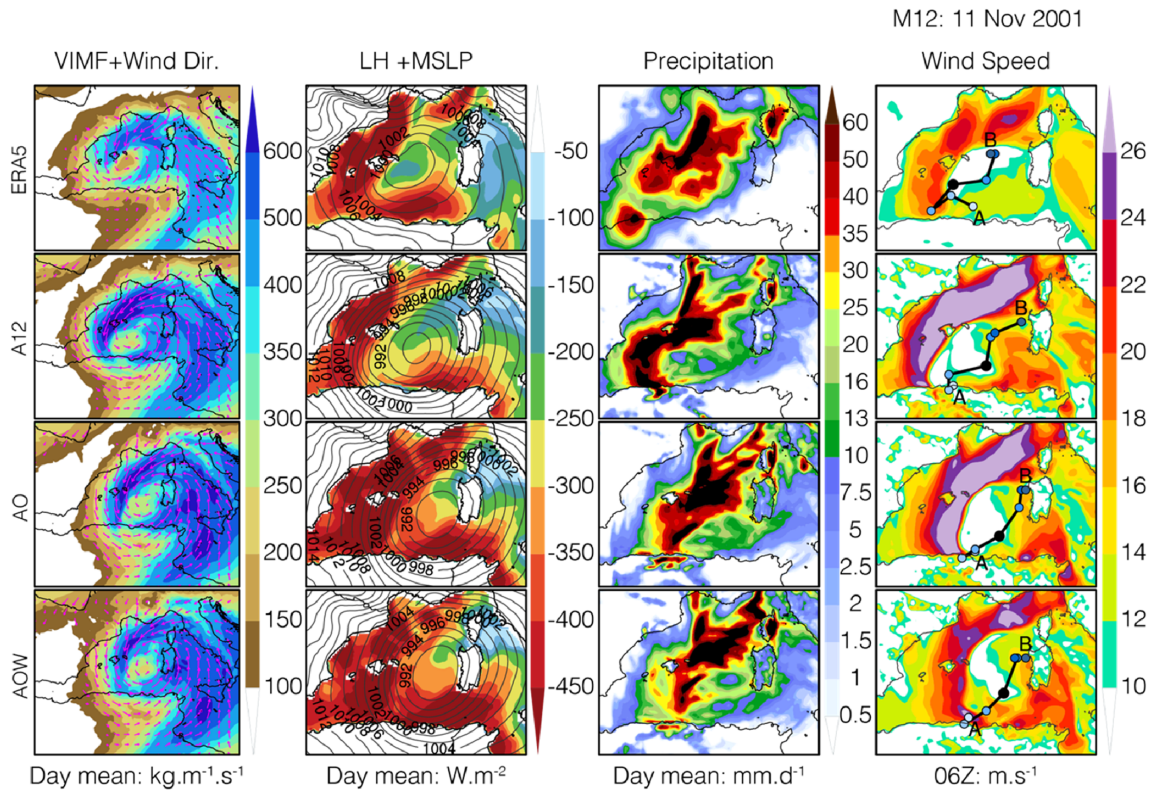

FIGURE 10 Same as in Figure 8, but for the 10–12 November 2001 medicane. [Colour figure can be viewed at wileyonlinelibrary.com]

overestimates mean and maximum latent heat flux, especially over the Gulf of Sidra, while AO (slightly) and A12 underestimate these values. Although A12 shows a better spatial distribution of wind speed (RMS error 3.08 $m \cdot s^{-1}$), AOW more accurately captures peak storm intensity at 19.33 $m \cdot s^{-1}$. All models maintain consistent wind strength representation with small mean biases. In terms of precipitation, AOW proves most accurate with the lowest average bias (0.2 $mm \cdot day^{-1}$), while A12 and AO underestimate rainfall (-2.36 $mm \cdot day^{-1}$ and -2.43 $mm \cdot day^{-1}$ respectively). The coupled simulations reveal interesting SST patterns as in ERA5 and GHRSST: neither shows cooling two days post-mature stage, and both match ERA5's SSTs at the mature stage despite reaching higher temperatures. A12, however, shows colder temperatures at the mature stage and continues cooling, though this is not reflected in latent heat fluxes. AOW's higher average wind speeds explain its increased latent heating compared to AO, despite similar SSTs. In the phase space diagrams, all datasets exhibit a cold to warm core transition, with simulations shifting from deep cold to shallow warm cores (Figure 13a). AOW uniquely follows ERA5's pattern by deepening its warm core, unlike A12 and AO. Although the AOW simulation provides the best results in terms of structure and amplitude, there is a slight eastward location shift. This shift may be due to reduced wind speed, which allows the system to develop an eye shape at its center by preserving the moisture gained when moving from dry land to the sea surface.

Figures S4–S7 present the remaining medicanes (M1, M2, M4, M5, M7, M8, M9, M10, M11, M13, M14, and M16) divided into two groups: autumn (Figures S4 and S5) and winter (Figures S6 and S7). All simulations closely resemble the reanalysis datasets in terms of moisture flux amounts in both seasons. However, the coupled simulations generally produce higher latent heat fluxes in both seasons compared to A12. SSTs are also higher in the AO and the AOW simulations during the mature stage of the medicanes and show similar values to the ERA5 dataset. The SST cooling two days after the mature stage is well -captured in autumn (or transition season) medicanes (Figure S5), which explains the higher latent heat fluxes in coupled simulations. In winter medicanes, while SST cooling is less pronounced, both AO and AOW simulations still show better alignment with the ERA5 dataset compared to A12 (Figure S7).

3.3 | Life cycle of medicanes

We analyze the life cycle of the four medicanes using key parameters at six-hourly intervals. Figure 14 displays

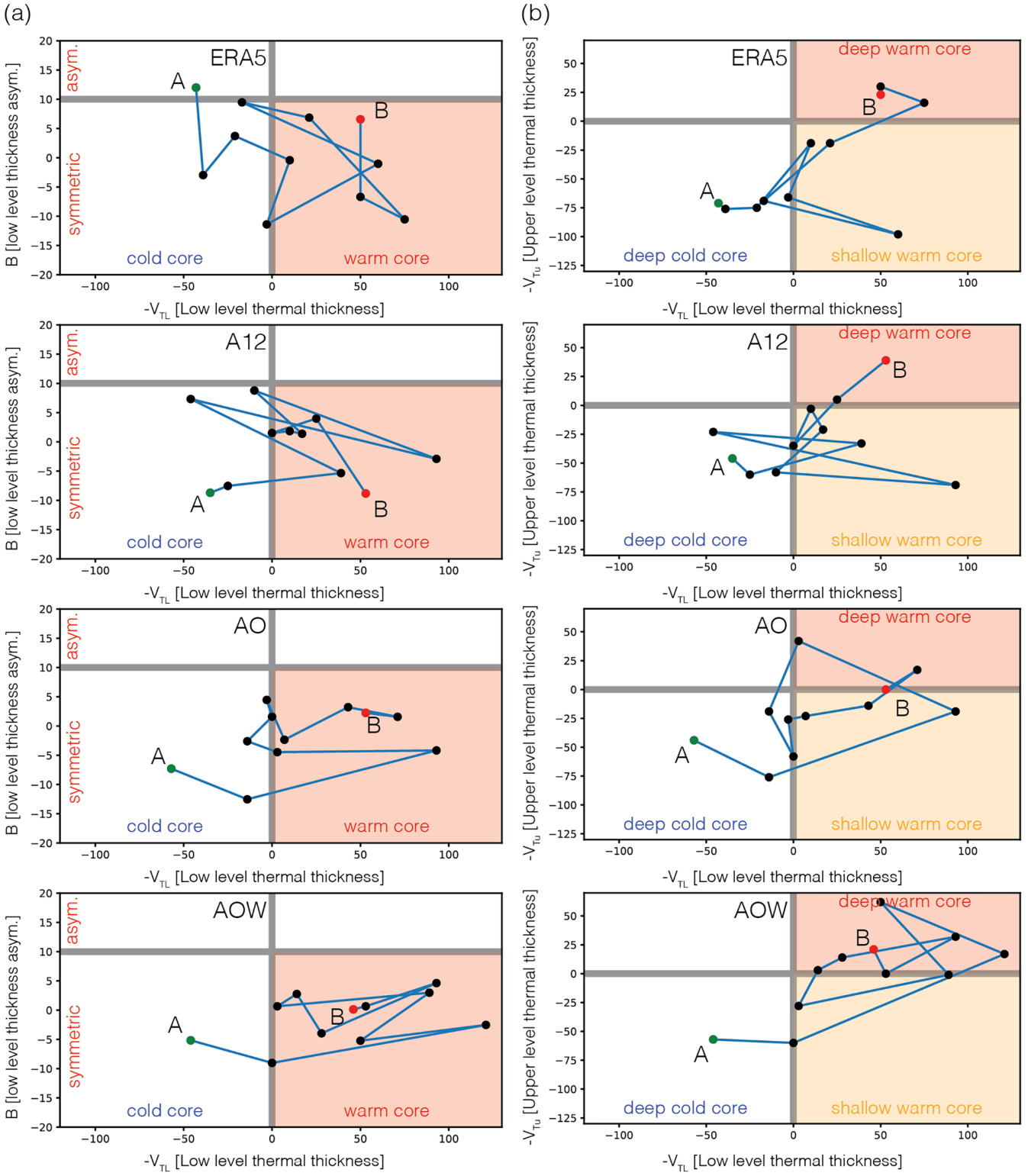

FIGURE 11 Same as in Figure 9 but for the10–12 November 2001 medicane. [Colour figure can be viewed at wileyonlinelibrary.com]

three variables: minimum sea level pressure (hPa), maximum wind speed ($m \cdot s^{-1}$), and maximum significant wave height (MH_s; m). For the statistical analysis, we identify maximum and minimum values within center-matched sub-regions and calculate root-mean-squared errors (RMSs) between the black dashed lines shown in Figure 14 (Table S3).

For the first case (M3), the mean sea level pressure and deepening produced by the AOW simulation are closer to ERA5 than those produced by the A12 and AO

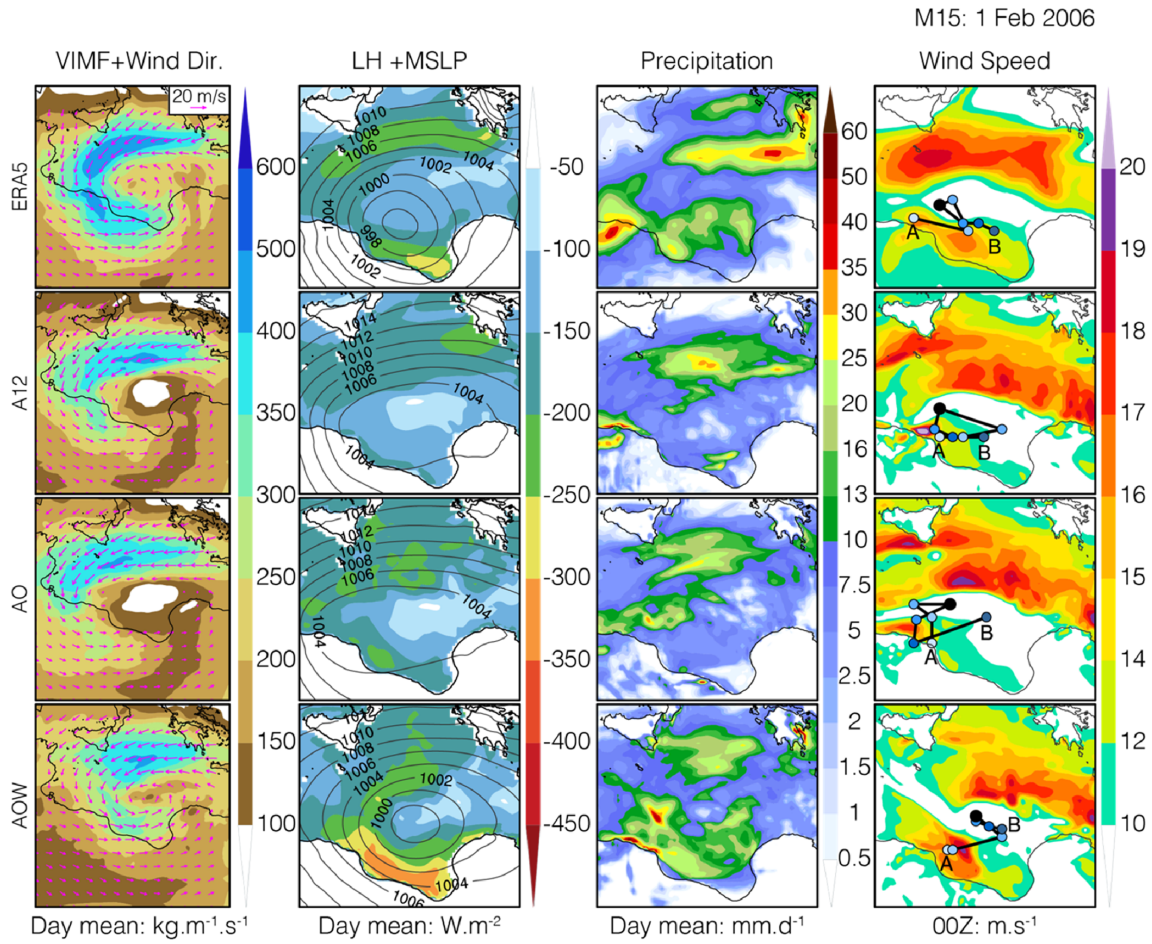

FIGURE 12 Same as in Figure 8, but for the 31 January–1 February 2006 medicane. [Colour figure can be viewed at wileyonlinelibrary.com]

simulations. However, the deepening is not as pronounced as in ERA5, and the timing of the minimum is delayed in all simulations. A12 does not show a life cycle at all. For maximum wind speed, the AO and AOW simulations produce values closer to the reanalysis, while the A12 simulation produces slightly higher values than the AO and AOW simulations (maximum wind speeds at the approximate mature stage: A12: 15.6 $m \cdot s^{-1}$, AO: 14.9 $m \cdot s^{-1}$, AOW: 14.8 $m \cdot s^{-1}$, ERA5: 14.9 $m \cdot s^{-1}$). Regarding MH_s, the W14 and AOW simulations produce very similar values of around ~14 $m \cdot s^{-1}$.

For medicane M6, the A12 simulation produces a mean sea level pressure of ~1008.9 hPa, while the AO and the AOW simulations produce deeper pressures (AO: 1006.5 hPa; AOW: 1004.5 hPa) that more closely match ERA5 reanalysis (1005.6 hPa). The AOW simulation reaches its minimum pressure slightly earlier than ERA5 and the other simulations. Both AO and AOW simulations accurately capture the changes in mean sea level pressure and deepening throughout the medicane's life cycle, though they overestimate maximum wind speeds as discussed earlier (Figure 8). The differences in mean sea level pressure and MH_ss between A12 and the coupled simulations can be attributed to A12's positioning over land during the mature phase, unlike ERA5 (shown in Figure 8).

M12 is an extremely intense medicane event, with ERA5 showing mean sea level pressure dropping to ~990 hPa. All simulations produce a stronger depression of approximately ~981 hPa, underestimating the mean sea level pressure. Although the simulations show similar mean sea level pressure values at the mature stage, the AOW simulation produces lower maximum wind speeds that more closely match the reanalysis data (RMS: 4.53 $m \cdot s^{-1}$). These reduced wind speeds in the AOW simulation consequently lead to lower MH_s values (RMS 1.71 $m \cdot s^{-1}$) compared to the W14 simulation (RMS: 4.09 $m \cdot s^{-1}$).

For the last medicane M15, both A12 and AO simulations develop a pressure minimum around 1000 hPa,

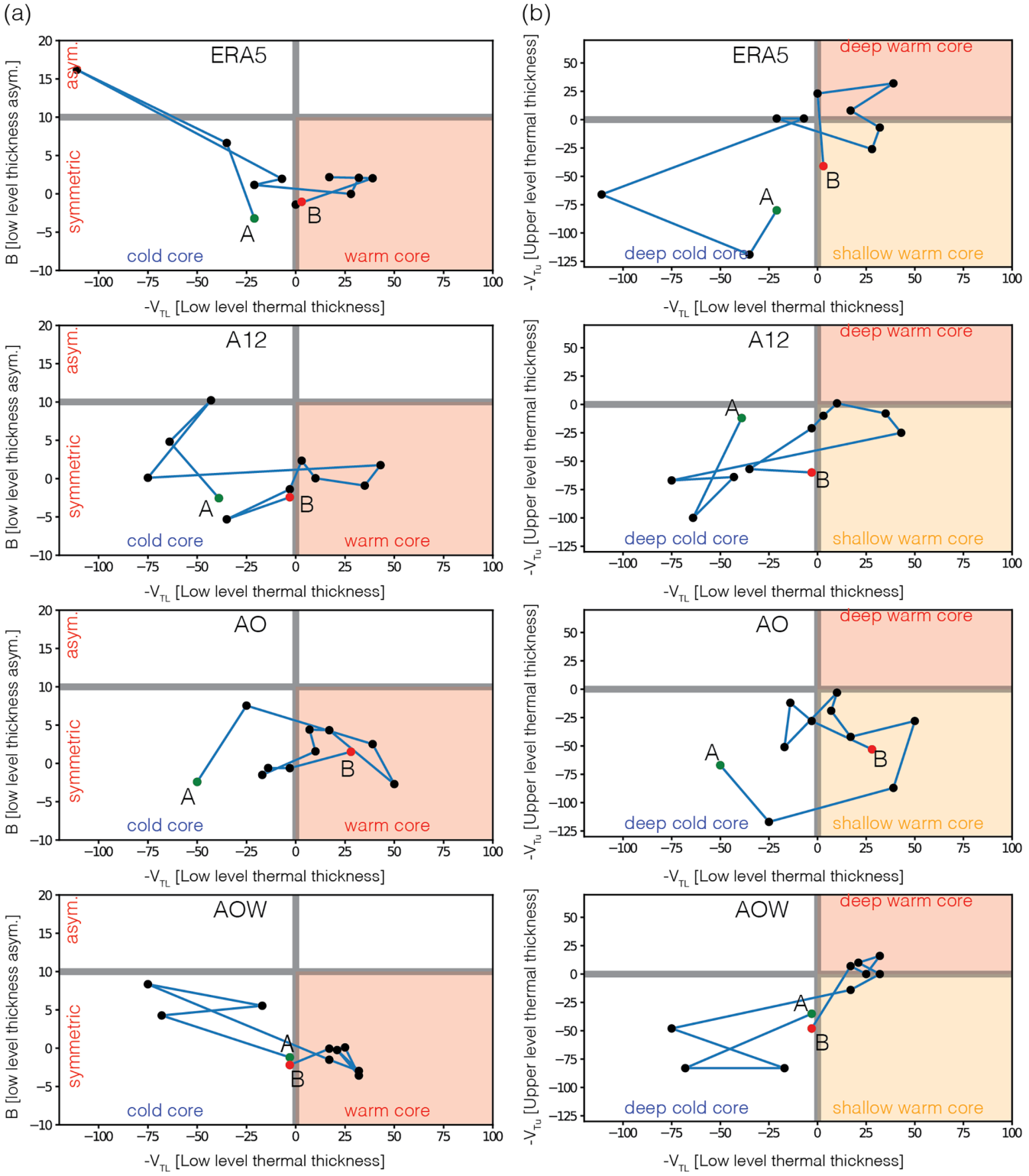

FIGURE 13 Same as in Figure 9, but for the 31 January–1 February 2006 medicane. [Colour figure can be viewed at wileyonlinelibrary.com]

while the AOW simulation produces a deeper pressure minimum around 997 hPa, which is closer to ERA5 (RMS: 3.53 hPa, compared to A12: 6.37 hPa and AO: 6.17 hPa). As noted earlier, the AOW simulation improves the storm symmetry, wind speed, and associated precipitation field. The timing of maximum wind speed varies

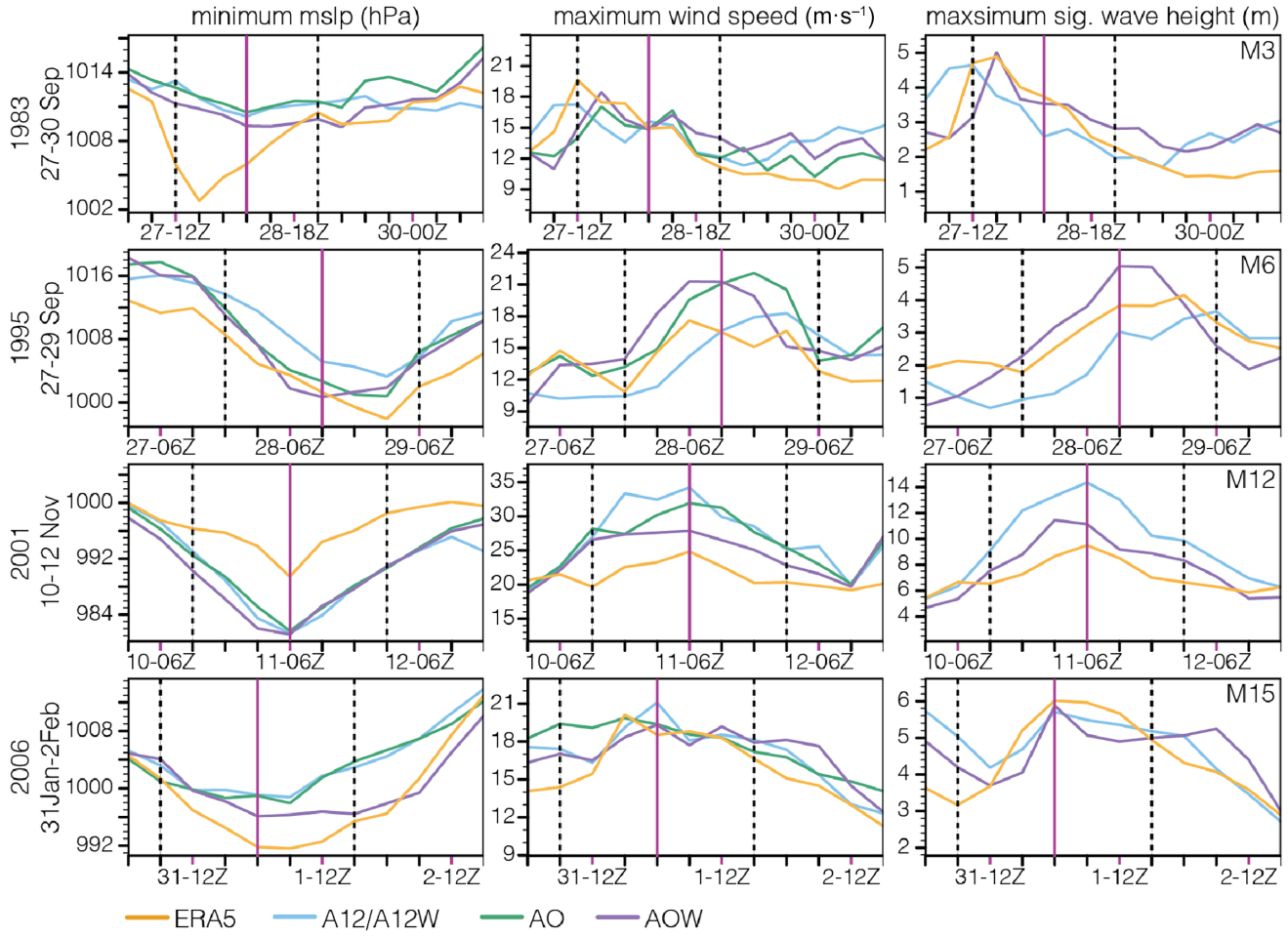

FIGURE 14 Time evolution of the sea level pressure minimum (in hPa), maximum wind speed (in m·s⁻) and maximum significant wave height (in m) of the selected medicane events. Horizontal dashed lines represent 18 hours prior to and from the minimum sea level pressure, and the horizontal solid line represents the approximate mature stage of the medicanes. [Colour figure can be viewed at wileyonlinelibrary.com]

among simulations and reanalyses, with AOW showing the lowest RMS (1.49 $m \cdot s^{-1}$), followed by A12 (1.71 $m \cdot s^{-1}$) and AO (2.38 $m \cdot s^{-1}$). The AOW simulation most closely matches the reanalyses during the mature stage. Figure 14 demonstrates that AOW's wind speeds best align with the reanalysis during this stage, even though the location of maximum wind speed differs. For maximum significant wave height (MH_s), both W14 and AOW simulations show similar values during the mature phase and throughout the medicane's life cycle (RMS values: A12: 0.80 m, AOW: 0.73 m).

In summary, we find that the pressure simulated by AOW performs better (lower RMS) in three cases while AO performs better in one case in medicanes' life cycle. For wind speeds, during the life cycle, both A12 and AOW perform better in two cases each. The AOW simulation consistently shows lower RMSs for MH_s than the W14.

4 | DISCUSSION

This study demonstrates that coupling atmospheric models with ocean and ocean–wave models improves the representation of medicanes compared to atmosphere-only (standalone) simulations in several aspects. Both coupled models exhibit a better representation of medicane tracks in the east–west direction, closely following reanalysis datasets. The inclusion of the wave model leads to reduced surface wind speeds through enhanced surface roughness lengths. In some cases, wave coupling enables medicane intensification through modified heat and momentum exchange between the ocean and the atmosphere – resulting in higher SSTs and increased latent heating. Previous studies also reported a decrease in low-level flow with wave coupling (Bouin *et al.*, 2017; Karagiorgos, 2024; Renault *et al.*, 2012; Ricchi

et al., 2017; Sauvage *et al.*, 2020; Varlas *et al.*, 2020). Reale *et al.* (2021) suggested that the internal variability in the Regional Climate Model (RCM) contributes to the eastward movement of cyclones. Additionally, Sanchez-Gomez and Somot (2018) demonstrated that in the Mediterranean region, when the same boundary conditions and RCM numerical settings are used with slightly different initial conditions, there is a higher variability in cyclone activity among different runs, particularly in the eastern part compared to the western part of the region. This can explain why some medicane events in the A12 simulation travel much faster towards the east than those in the AOW model (e.g., 27–29 September 1995 event [M6]).

Another important point regarding medicanes is the fundamental role of SSTs in their formation processes, as reported in many studies (Miglietta *et al.*, 2011; Pytharoulis, 2018; Ricchi *et al.*, 2017, 2019), with several recommending coupled models. Our analysis shows that both AOW and AO simulations typically produce higher SST values compared to A12 and more closely match ERA5 and GHRSST data, particularly for autumn medicanes. These higher SSTs lead to increased evaporation and fuel the storm with increased heat and momentum fluxes, as observed in the 10–12 November 2001 event (M12). While this helps to intensify the medicanes to match ERA5 data in most cases, it occasionally increases the duration of the deep warm core phase.

In both autumn and winter medicanes, latent heat fluxes are higher in coupled models, particularly in the AOW simulation. Coupled simulations show a marked improvement in capturing SST cooling two days after the mature state compared to the A12 simulation, especially for fall medicanes. This improvement is evident when compared to ERA5 data. Winter medicanes exhibit a similar trend, with coupled models better representing cooling than A12, though the SST cooling is less pronounced after these events. This seasonal variation can be attributed to different driving processes. Winter medicanes are largely influenced by dynamic effects and systems originating from the Atlantic (Batibeniz *et al.*, 2020), primarily driven by external forcing through wind strength. In contrast, during the transition seasons, thermodynamic effects such as local recycling (Batibeniz *et al.*, 2020) play a more significant role in medicane development.

The intensity and dynamics of medicanes are influenced by both diabatic processes and baroclinic forcing. When one factor diminishes, the other becomes more prominent (Flaounas *et al.*, 2021; Reale *et al.*, 2021). The air–sea interaction plays an important role in both processes. For medicanes driven by diabatic processes, warm ocean waters serve as the primary energy source and increase the air–sea heat exchanges (Darmaraki *et al.*, 2019; Soto-Navarro *et al.*, 2020). This process fuels convection through evaporation, providing the required moisture as exemplified in the case from 10 to 12 November 2001 (M12), which is investigated in our study. For baroclinically driven medicanes, surface waves develop due to the cyclone's rotation and rapidly changing surface winds. These waves influence air–sea interactions by modifying surface roughness, which affects the momentum and heat exchange between the ocean and atmosphere. Increased surface roughness enhances surface stress while reducing wind speed at the sea surface (Persson *et al.*, 2009). Despite this decrease in near-surface wind speed, the enhanced roughness increases surface sensible and latent heat fluxes (Persson *et al.*, 2009). As a result, turbulent kinetic energy and eddy mixing coefficients increase, boosting the vertical transport of heat, momentum, and moisture. This changes the pressure gradient near the cyclone center and intensifies the low-level frontal intensity. This can explain why we find increased latent heat fluxes in the 31 January–1 February 2006 case (M15) despite decreased wind speed.

5 | CONCLUSIONS

Using four different simulations to reproduce medicanes, we provide information regarding the possible effects of air–sea interaction and the added value of coupled modeling. Our results reveal that coupling the ocean provides better storm intensity through interactive SST input. In some cases, evaporation increases depending on the warmer SSTs produced by the coupled models (generally in line with ERA5), which enhances the latent heat flux and develops better intensity. The standalone model mostly underestimates SSTs, causing an underestimation of the latent heat fluxes. This leads storms to produce higher minimum mean sea level pressures.

Our results also show that using a coupled model with the wave component helps produce a better eyewall at the center of the medicane, which is a measure of strength in the system and demonstrates its tropical features. Without coupling to surface waves, simulations overestimate the surface wind speed, even though the sea level pressure may be close to reanalyses in some cases. Combining this with the underestimation of SSTs in the A12 simulation, the system appears stronger due to higher winds but does not develop vertically because of underrepresented heat and momentum fluxes. In contrast, AOW cyclones are usually deeper compared to A12 but do not necessarily have higher winds. In cases where both coupled models show similar wind fields and SSTs, the higher latent heat in AOW is due to increased roughness length, which

makes the system deeper and creates the characteristic eye shape.

A notable limitation of this study is the resolution of the Med-CORDEX configuration (12 km atmosphere, ~9 km ocean), which constrains our ability to fully capture fine-scale atmospheric and oceanic processes and their feedback to cyclone dynamics. Previous studies, such as Cioni *et al.* (2018) and Pantillon *et al.* (2024), have shown that resolutions of 2 km or finer may be necessary to accurately resolve the internal structure of cyclones and the processes that drive their intensification. Similarly, as demonstrated by Sanna *et al.* (2013), ocean model resolution plays a critical role in representing mesoscale features like eddies, which are crucial for accurately simulating cyclogenesis. While our simulations are capable of reproducing broad-scale dynamics and ocean surface cooling associated with cyclone passage, the coarser resolution may lead to some underrepresentation of sub-mesoscale interactions. Future studies would benefit from higher-resolution simulations to better resolve these processes, though such simulations remain computationally demanding. Despite these limitations, our comparison with ERA5 and GHRSST data suggests that the model provides a reasonable representation of ocean surface cooling associated with cyclone passage – a key aspect of ocean–atmosphere coupling central to this study.

Overall, our study demonstrates the importance of air–sea interactions and the dynamics of oceanic and atmospheric processes in reducing model simulation uncertainties. It enhances our understanding of the feedback mechanisms between the atmosphere and ocean during medicane events, though further analysis is required to understand the influence of air–sea interaction on upper-level forces. With sufficient computational resources, coupled models should be prioritized to accurately capture momentum and heat fluxes between the ocean and atmosphere, as these more comprehensive simulations provide critical insights for flood risk assessments and coastal management strategies in regions vulnerable to medicane impacts.

ACKNOWLEDGEMENTS

This study has been supported by a research grant 40248 by the Istanbul Technical University (ITU) and a research grant (116Y136) provided by The Scientific and Technological Research Council of Turkey (TUBITAK). The computing resources used in this work were provided by the National Center for High Performance Computing (UHEM), Turkey under grant number 5004782017. Ufuk Utku Turuncoglu was supported by the National Center for Atmospheric Research, which is a major facility sponsored by the National Science Foundation under Cooperative Agreement No. 1852977. Christoph C. Raible is supported by the Swiss National Science Foundation (SNF) within the project HARPYIE grant no. IZCOZ0_205416. We would like to thank two anonymous reviewers for their careful reading of our manuscript and their insightful comments and suggestions.. Open access publishing facilitated by Universitat Bern, as part of the Wiley - Universitat Bern agreement via the Consortium Of Swiss Academic Libraries.

FUNDING INFORMATION

This study has been supported by a research grant 40248 by the Istanbul Technical University (ITU) and a research grant (116Y136) provided by The Scientific and Technological Research Council of Turkey (TUBITAK). The computing resources used in this work were provided by the National Center for High Performance Computing (UHEM), Turkey under grant number 5004782017. Ufuk Utku Turuncoglu was supported by the National Center for Atmospheric Research, which is a major facility sponsored by the National Science Foundation under Cooperative Agreement No. 1852977. Christoph C. Raible is supported by the Swiss National Science Foundation (SNF) within the project HARPYIE grant no. IZCOZ0_205416.

DATA AVAILABILITY STATEMENT

The simulations used in this study were produced by the first author (FB) and are available upon request. All reanalysis and observational data used are open-source and accessible online. Detailed information on data sources and access procedures can be provided upon reasonable request.

ORCID

Fulden Batibeniz https://orcid.org/0000-0002-1751-3385
Barış Önol https://orcid.org/0000-0002-6382-7975
Ufuk Utku Turuncoglu https://orcid.org/0000-0001-5499-7326
Christoph C. Raible https://orcid.org/0000-0003-0176-0602

REFERENCES

Akhtar, N., Brauch, J., Dobler, A., Béranger, K. & Ahrens, B. (2014) Medicanes in an ocean–atmosphere coupled regional climate model. *Natural Hazards and Earth System Sciences*, 14(8), 2189–2201. Available from: https://doi.org/10.5194/nhess-14-2189-2014

Amante, C. & Eakins, B.W. (2009) *ETOPO1 Global Relief Model converted to PanMap layer format* [dataset]. NOAA-National Geophysical Data Center, PANGAEA.

Antonov, J.I., Seidov, D., Boyer, T.P., Locarnini, R.A., Mishonov, A.V., Garcia, H.E. et al. (2010) World ocean atlas 2009, Volume 2: Salinity. (Levitus, Ed., NOAA Atlas NESDIS 69, U.S. Government Printing Office, Washington, D.C.,). 184 pp.

Arreola, J.L., Homar, V., Romero, R., Ramis, C. & Alonso, S. (2003) Multiscale numerical study of the 10-12 November 2001 strong cyclogenesis event in the Western Mediterranean. Sec. 1 Num 30.

Batibeniz, F., Ashfaq, M., Önol, B., Turuncoglu, U.U., Mehmood, S. & Evans, K.J. (2020) Identification of major moisture sources across the Mediterranean Basin. *Climate Dynamics*, 54(9–10), 4109–4127. Available from: https://doi.org/10.1007/s00382-020-05224-3

Bouin, M.-N. & Lebeaupin Brossier, C. (2020) Surface processes in the 7 November 2014 medicane from air–sea coupled high-resolution numerical modelling. *Atmospheric Chemistry and Physics*, 20(11), 6861–6881. Available from: https://doi.org/10.5194/acp-20-6861-2020

Bouin, M.-N., Redelsperger, J.-L. & Lebeaupin Brossier, C. (2017) Processes leading to deep convection and sensitivity to sea-state representation during HyMeX IOP8 heavy precipitation event. *Quarterly Journal of the Royal Meteorological Society*, 143(707), 2600–2615. Available from: https://doi.org/10.1002/qj.3111

Carrió, D.S., Homar, V., Jansa, A., Romero, R. & Picornell, M.A. (2017) Tropicalization process of the 7 November 2014 Mediterranean cyclone: numerical sensitivity study. *Atmospheric Research*, 197, 300–312. Available from: https://doi.org/10.1016/j.atmosres.2017.07.018

Cavaleri, L., Barbariol, F. & Benetazzo, A. (2020) Wind–wave modeling: where we are, where to go. *Journal of Marine Science and Engineering*, 8(4), 260. Available from: https://doi.org/10.3390/jmse8040260

Cavicchia, L. & Von Storch, H. (2012) The simulation of medicanes in a high-resolution regional climate model. *Climate Dynamics*, 39(9–10), 2273–2290. Available from: https://doi.org/10.1007/s00382-011-1220-0

Cavicchia, L., Von Storch, H. & Gualdi, S. (2014a) A long-term climatology of medicanes. *Climate Dynamics*, 43(5–6), 1183–1195. Available from: https://doi.org/10.1007/s00382-013-1893-7

Cavicchia, L., Von Storch, H. & Gualdi, S. (2014b) Mediterranean tropical-like cyclones in present and future climate. *Journal of Climate*, 27(19), 7493–7501. Available from: https://doi.org/10.1175/JCLI-D-14-00339.1

Chaboureau, J., Pantillon, F., Lambert, D., Richard, E. & Claud, C. (2012) Tropical transition of a Mediterranean storm by jet crossing. *Quarterly Journal of the Royal Meteorological Society*, 138(664), 596–611. Available from: https://doi.org/10.1002/qj.960

Chen, S.S. & Curcic, M. (2016) Ocean surface waves in hurricane Ike (2008) and Superstorm Sandy (2012): coupled model predictions and observations. *Ocean Modelling*, 103, 161–176. Available from: https://doi.org/10.1016/j.ocemod.2015.08.005

Chen, S.S., Zhao, W., Donelan, M.A. & Tolman, H.L. (2013) Directional wind–wave coupling in fully coupled atmosphere–Wave–Ocean models: results from CBLAST-hurricane. *Journal of the Atmospheric Sciences*, 70(10), 3198–3215. Available from: https://doi.org/10.1175/JAS-D-12-0157.1

Cioni, G., Cerrai, D. & Klocke, D. (2018) Investigating the predictability of a Mediterranean tropical-like cyclone using a storm-resolving model. *Quarterly Journal of the Royal Meteorological Society*, 144(714), 1598–1610. Available from: https://doi.org/10.1002/qj.3322

Claud, C., Alhammoud, B., Funatsu, B.M. & Chaboureau, J.-P. (2010) Mediterranean hurricanes: large-scale environment and convective and precipitating areas from satellite microwave observations. *Natural Hazards and Earth System Science*, 10(10), 2199–2213. Available from: https://doi.org/10.5194/nhess-10-2199-2010

Dafis, S., Claud, C., Kotroni, V., Lagouvardos, K. & Rysman, J. (2020) Insights into the convective evolution of Mediterranean tropical-like cyclones. *Quarterly Journal of the Royal Meteorological Society*, 146(733), 4147–4169. Available from: https://doi.org/10.1002/qj.3896

Darmaraki, S., Somot, S., Sevault, F., Nabat, P., Cabos Narvaez, W.D., Cavicchia, L. et al. (2019) Future evolution of marine heatwaves in the Mediterranean Sea. *Climate Dynamics*, 53(3–4), 1371–1392. Available from: https://doi.org/10.1007/s00382-019-04661-z

Davison, S., Benetazzo, A., Barbariol, F., Ricchi, A. & Ferretti, R. (2024) Characterization of extreme wave fields during Mediterranean tropical-like cyclones. *Frontiers in Marine Science*, 10, 1268830. Available from: https://doi.org/10.3389/fmars.2023.1268830

Davolio, S., Miglietta, M.M., Moscatello, A., Pacifico, F., Buzzi, A. & Rotunno, R. (2009) Numerical forecast and analysis of a tropical-like cyclone in the Ionian Sea. *Natural Hazards and Earth System Sciences*, 9(2), 551–562. Available from: https://doi.org/10.5194/nhess-9-551-2009

Dickinson, R.E., Errico, R.M., Giorgi, F. & Bates, G.T. (1989) A regional climate model for the western United States. *Climatic Change*, 15(3), 383–422. Available from: https://doi.org/10.1007/BF00240465

Emanuel, K. (2005) Genesis and maintenance of "Mediterranean hurricanes". *Advances in Geosciences*, 2, 217–220. Available from: https://doi.org/10.5194/adgeo-2-217-2005

Emanuel, K.A. (1991) A scheme for representing cumulus convection in Large-scale models. *Journal of the Atmospheric Sciences*, 48(21), 2313–2329. Available from: https://doi.org/10.1175/1520-0469(1991)048<2313:ASFRCC>2.0.CO;2

Emanuel, K.A. & Živković-Rothman, M. (1999) Development and evaluation of a convection scheme for use in climate models. *Journal of the Atmospheric Sciences*, 56(11), 1766–1782. Available from: https://doi.org/10.1175/1520-0469(1999)056<1766:DAEOAC>2.0.CO;2

Fichaut, M., Garcia, M.J., Giorgetti, A., Iona, A., Kuznetsov, A., Rixen, M. et al. (2003) MEDAR/MEDATLAS 2002: a Mediterranean and Black Sea database for operational oceanography. In: Dahlin, H., Flemming, N.C., Nittis, K. & Petersson, S.E. (Eds.) *Building the European capacity in operational oceanography*, Vol. 69. Elsevier, pp. 645–648.

Fita, L. & Flaounas, E. (2018) Medicanes as subtropical cyclones: the December 2005 case from the perspective of surface pressure tendency diagnostics and atmospheric water budget. *Quarterly Journal of the Royal Meteorological Society*, 144(713), 1028–1044. Available from: https://doi.org/10.1002/qj.3273

Fita, L., Romero, R., Luque, A., Emanuel, K. & Ramis, C. (2007) Analysis of the environments of seven Mediterranean tropical-like storms using an axisymmetric, nonhydrostatic, cloud resolving model. *Natural Hazards and Earth System Sciences*, 7(1), 41–56. Available from: https://doi.org/10.5194/nhess-7-41-2007

Fita, L., Romero, R., Luque, A. & Ramis, C. (2009) Effects of assimilating precipitation zones derived from satellite and lightning data on numerical simulations of tropical-like Mediterranean storms. *Annales Geophysicae*, 27(8), 3297–3319. Available from: https://doi.org/10.5194/angeo-27-3297-2009

Flaounas, E., Davolio, S., Raveh-Rubin, S., Pantillon, F., Miglietta, M.M., Gaertner, M.A. et al. (2022) Mediterranean cyclones: current knowledge and open questions on dynamics, prediction, climatology and impacts. *Weather and Climate Dynamics*, 3(1), 173–208. Available from: https://doi.org/10.5194/wcd-3-173-2022

Flaounas, E., Fita, L., Lagouvardos, K. & Kotroni, V. (2019) Heavy rainfall in Mediterranean cyclones, part II: water budget, precipitation efficiency and remote water sources. *Climate Dynamics*, 53(5–6), 2539–2555. Available from: https://doi.org/10.1007/s00382-019-04639-x

Flaounas, E., Gray, S.L. & Teubler, F. (2021) A process-based anatomy of Mediterranean cyclones: from baroclinic lows to tropical-like systems. *Weather and Climate Dynamics*, 2(1), 255–279. Available from: https://doi.org/10.5194/wcd-2-255-2021

Flaounas, E., Kelemen, F.D., Wernli, H., Gaertner, M.A., Reale, M., Sanchez-Gomez, E. et al. (2018) Assessment of an ensemble of ocean–atmosphere coupled and uncoupled regional climate models to reproduce the climatology of Mediterranean cyclones. *Climate Dynamics*, 51(3), 1023–1040. Available from: https://doi.org/10.1007/s00382-016-3398-7

Giorgi, F., Coppola, E., Solmon, F., Mariotti, L., Sylla, M., Bi, X. et al. (2012) RegCM4: model description and preliminary tests over multiple CORDEX domains. *Climate Research*, 52, 7–29. Available from: https://doi.org/10.3354/cr01018

Giorgi, F., Jones, C. & Asrar, G.R. (2009) Addressing climate information needs at the regional level: the CORDEX framework. *World Meteorological Organization (WMO) Bulletin*, 58(3), 175.

Hagemann, S. & Dümenil, L. (1997) A parametrization of the lateral waterflow for the global scale. *Climate Dynamics*, 14(1), 17–31. Available from: https://doi.org/10.1007/s003820050205

Hagemann, S. & Gates, L.D. (2001) Validation of the hydrological cycle of ECMWF and NCEP reanalyses using the MPI hydrological discharge model. *Journal of Geophysical Research: Atmospheres*, 106(D2), 1503–1510. Available from: https://doi.org/10.1029/2000JD900568

Haidvogel, D.B., Arango, H., Budgell, W.P., Cornuelle, B.D., Curchitser, E., Di Lorenzo, E. et al. (2008) Ocean forecasting in terrain-following coordinates: formulation and skill assessment of the Regional Ocean modeling system. *Journal of Computational Physics*, 227(7), 3595–3624. Available from: https://doi.org/10.1016/j.jcp.2007.06.016

Hart, R.E. (2003) A cyclone phase space derived from thermal wind and thermal asymmetry. *Monthly Weather Review*, 131(4), 585–616. Available from: https://doi.org/10.1175/1520-0493(2003)131<0585:ACPSDF>2.0.CO;2

Hersbach, H., Bell, B., Berrisford, P., Hirahara, S., Horányi, A., Muñoz-Sabater, J. et al. (2020) The ERA5 global reanalysis. *Quarterly Journal of the Royal Meteorological Society*, 146(730), 1999–2049. Available from: https://doi.org/10.1002/qj.3803

Holtslag, A.A.M., De Bruijn, E.I.F. & Pan, H.-L. (1990) A high resolution air mass transformation model for short-range weather forecasting. *Monthly Weather Review*, 118(8), 1561–1575. Available from: https://doi.org/10.1175/1520-0493(1990)118<1561:AHRAMT>2.0.CO;2

Homar, V. & Stensrud, D.J. (2004) Sensitivities of an intense Mediterranean cyclone: analysis and validation. *Quarterly Journal of the Royal Meteorological Society*, 130(602), 2519–2540. Available from: https://doi.org/10.1256/qj.03.85

Homar, V., Romero, R., Stensrud, D.J., Ramis, C. & Alonso, S. (2003) Numerical diagnosis of a small, quasi-tropical cyclone over the western Mediterranean: Dynamical vs. boundary factors. *Quarterly Journal of the Royal Meteorological Society*, 129(590), 1469–1490. Available from: https://doi.org/10.1256/qj.01.91

Homar, V., Ramis, C. & Alonso, S. (2002) A deep cyclone of African origin over the Western Mediterranean: diagnosis and numerical simulation. *Annales Geophysicae*, 20(1), 93–106. Available from: https://doi.org/10.5194/angeo-20-93-2002

Hwang, P.A. (2016) Fetch- and duration-limited nature of surface wave growth inside tropical cyclones: with applications to Air–Sea exchange and remote sensing. *Journal of Physical Oceanography*, 46(1), 41–56. Available from: https://doi.org/10.1175/JPO-D-15-0173.1

Janssen, P.A.E.M. (2008) Progress in ocean wave forecasting. *Journal of Computational Physics*, 227(7), 3572–3594. Available from: https://doi.org/10.1016/j.jcp.2007.04.029

Karagiorgos, J. (2024) Ocean-wave-atmosphere coupling effect in Medicane forecasting. *Atmospheric Research*, 304, 107418.

Katsafados, P., Papadopoulos, A., Korres, G. & Varlas, G. (2016) A fully coupled atmosphere–ocean wave modeling system for the Mediterranean Sea: interactions and sensitivity to the resolved scales and mechanisms. *Geoscientific Model Development*, 9(1), 161–173. Available from: https://doi.org/10.5194/gmd-9-161-2016

Kerkmann, J. & Bachmeier, S. (2011) Development of a tropical storm in the Mediterranean Sea (6-9 November 2011).

Kiehl, J.T., Hack, J.J., Bonan, G.B., Boville, B.A., Briegleb, B.P., Williamson, D.L. et al. (1996) Description of the NCAR Community Climate Model (CCM3). 159.

Kuo, Y.H., Guo, Y.R. & Reed, R.J. (2002) *Simulation of a mesoscale cyclone over the Mediterranean Sea*. University Corporation for Atmospheric Research, Boulder, CO.

Large, W.G., McWilliams, J.C. & Doney, S.C. (1994) Oceanic vertical mixing: a review and a model with a nonlocal boundary layer parameterization. *Reviews of Geophysics*, 32(4), 363–403. Available from: https://doi.org/10.1029/94RG01872

Levizzani, V., Laviola, S., Malvaldi, A. & Cattani, E. (2012) *Severe storms over the Mediterranean Sea: a satellite and model analysis*. Brazil: Institute of Atmospheric Sciences and Climate.

Liberti, L., Carillo, A. & Sannino, G. (2013) Wave energy resource assessment in the Mediterranean, the Italian perspective. *Renewable Energy*, 50, 938–949. Available from: https://doi.org/10.1016/j.renene.2012.08.023

Lionello, P., Bhend, J., Buzzi, A., Della-Marta, P.M., Krichak, S.O., Jansà, A. et al. (2006) Chapter 6 cyclones in the Mediterranean region: climatology and effects on the environment. In:

Developments in earth and environmental sciences, Vol. 4. Elsevier, pp. 325–372.

Lionello, P., Cogo, S., Galati, M.B. & Sanna, A. (2008) The Mediterranean surface wave climate inferred from future scenario simulations. *Global and Planetary Change*, 63(2–3), 152–162. Available from: https://doi.org/10.1016/j.gloplacha.2008.03.004

Lionello, P., Martucci, G. & Zampieri, M. (2003) Implementation of a coupled atmosphere-Wave-Ocean model in the Mediterranean Sea: sensitivity of the short time scale evolution to the Air-Sea coupling mechanisms. *Journal of Atmospheric & Ocean Science*, 9(1–2), 65–95. Available from: https://doi.org/10.1080/1023673031000151421

Locarnini, R.A., Mishonov, A.V., Antonov, J.I., Boyer, T.P., Garcia, H.E., Baranova, O.K. et al. (2010) World ocean atlas 2009, Volume 1: Temperature. (Levitus, Ed., NOAA Atlas NESDIS 68, U.S. Government Printing Office, Washington, D.C.,). 184 pp.

Marshall, J., Adcroft, A., Hill, C., Perelman, L. & Heisey, C. (1997a) A finite-volume, incompressible Navier stokes model for studies of the ocean on parallel computers. *Journal of Geophysical Research: Oceans*, 102(C3), 5753–5766. Available from: https://doi.org/10.1029/96JC02775

Marshall, J., Hill, C., Perelman, L. & Adcroft, A. (1997b) Hydrostatic, quasi-hydrostatic, and nonhydrostatic ocean modeling. *Journal of Geophysical Research: Oceans*, 102(C3), 5733–5752. Available from: https://doi.org/10.1029/96JC02776

Messmer, M., Gómez-Navarro, J.J. & Raible, C.C. (2017) Sensitivity experiments on the response of Vb cyclones to sea surface temperature and soil moisture changes. *Earth System Dynamics*, 8(3), 477–493. Available from: https://doi.org/10.5194/esd-8-477-2017

Miglietta, M.M., Laviola, S., Malvaldi, A., Conte, D., Levizzani, V. & Price, C. (2013) Analysis of tropical-like cyclones over the Mediterranean Sea through a combined modeling and satellite approach. *Geophysical Research Letters*, 40(10), 2400–2405. Available from: https://doi.org/10.1002/grl.50432

Miglietta, M.M., Mastrangelo, D. & Conte, D. (2015) Influence of physics parameterization schemes on the simulation of a tropical-like cyclone in the Mediterranean Sea. *Atmospheric Research*, 153, 360–375. Available from: https://doi.org/10.1016/j.atmosres.2014.09.008

Miglietta, M.M., Moscatello, A., Conte, D., Mannarini, G., Lacorata, G. & Rotunno, R. (2011) Numerical analysis of a Mediterranean 'hurricane' over south-eastern Italy: sensitivity experiments to sea surface temperature. *Atmospheric Research*, 101(1–2), 412–426. Available from: https://doi.org/10.1016/j.atmosres.2011.04.006

Miglietta, M.M. & Rotunno, R. (2019) Development mechanisms for Mediterranean tropical-like cyclones (medicanes). *Quarterly Journal of the Royal Meteorological Society*, 145(721), 1444–1460. Available from: https://doi.org/10.1002/qj.3503

Monbaliu, J., Padilla-Hernández, R., Hargreaves, J.C., Albiach, J.C.C., Luo, W., Sclavo, M. et al. (2000) The spectral wave model, WAM, adapted for applications with high spatial resolution. *Coastal Engineering*, 41(1–3), 41–62. Available from: https://doi.org/10.1016/S0378-3839(00)00026-0

Moscatello, A., Miglietta, M.M. & Rotunno, R. (2008) Numerical analysis of a Mediterranean "hurricane" over southeastern Italy. *Monthly Weather Review*, 136(11), 4373–4397. Available from: https://doi.org/10.1175/2008MWR2512.1

Mylonas, M., Douvis, K., Polychroni, I., Politi, N. & Nastos, P. (2019) Analysis of a Mediterranean tropical-like cyclone. Sensitivity to WRF parameterizations and horizontal resolution. *Atmosphere*, 10(8), 425. Available from: https://doi.org/10.3390/atmos10080425

Nastos, P.T., Karavana Papadimou, K. & Matsangouras, I.T. (2018) Mediterranean tropical-like cyclones: impacts and composite daily means and anomalies of synoptic patterns. *Atmospheric Research*, 208, 156–166. Available from: https://doi.org/10.1016/j.atmosres.2017.10.023

Nykjaer, L. (2009) Mediterranean Sea surface warming 1985–2006. *Climate Research*, 39(1), 11–17.

Pal, J., Small, E. & Eltahir, E. (2000) Simulation of regional-scale water and energy budgets: representation of subgrid cloud and precipitation processes within RegCM. *Journal of Geophysical Research*, 105, 29579–29594. Available from: https://doi.org/10.1029/2000JD900415

Pantillon, F., Davolio, S., Avolio, E., Calvo-Sancho, C., Carrió, D.S., Dafis, S. et al. (2024) The crucial representation of deep convection for the cyclogenesis of Medicane Ianos. *Weather and Climate Dynamics*, 5(3), 1187–1205. Available from: https://doi.org/10.5194/wcd-5-1187-2024

Pastor, F., Valiente, J.A. & Khodayar, S. (2020) A warming Mediterranean: 38 years of increasing sea surface temperature. *Remote Sensing*, 12(17), 2687. Available from: https://doi.org/10.3390/rs12172687

Persson, P.O., Hare, J.E., Nance, L.B. & Walter, B. (2009) Impact of air-sea interactions on extra-tropical cyclones. In: ECMWF Workshop on Ocean-Atmosphere Interactions, 10-12 November 2008, 123–146.

Picornell, M.A., Campins, J. & Jansà, A. (2014) Detection and thermal description of medicanes from numerical simulation. *Natural Hazards and Earth System Sciences*, 14(5), 1059–1070. Available from: https://doi.org/10.5194/nhess-14-1059-2014

Powers, J.G., Klemp, J.B., Skamarock, W.C., Davis, C.A., Dudhia, J., Gill, D.O. et al. (2017) The weather research and forecasting model: overview, system efforts, and future directions. *Bulletin of the American Meteorological Society*, 98(8), 1717–1737. Available from: https://doi.org/10.1175/BAMS-D-15-00308.1

Pytharoulis, I. (2018) Analysis of a Mediterranean tropical-like cyclone and its sensitivity to the sea surface temperatures. *Atmospheric Research*, 208, 167–179. Available from: https://doi.org/10.1016/j.atmosres.2017.08.009

Pytharoulis, I., Craig, G. & Ballard, S. (2000) The hurricane-like Mediterranean cyclone of January 1995. *Meteorological Applications*, 7(3), 261–279. Available from: https://doi.org/10.1017/S1350482700001511

Rasmussen, E. & Zick, C. (1987) A subsynoptic vortex over the Mediterranean with some resemblance to polar lows. *Tellus A: Dynamic Meteorology and Oceanography*, 39(4), 408–425. Available from: https://doi.org/10.3402/tellusa.v39i4.11770

Ramis, C., Tous, M., Homar, V., Romero, R. & Alonso, S. (2013) Medicanes: quasi-tropical mesoscale cyclones in the Mediterranean. *Adverse Weather in Spain*, 34.

Reale, M., Cabos Narvaez, W.D., Cavicchia, L., Conte, D., Coppola, E., Flaounas, E. et al. (2021) Future projections of Mediterranean cyclone characteristics using the med-CORDEX

ensemble of coupled regional climate system models. *Climate Dynamics*, 58, 1–24. Available from: https://doi.org/10.1007/s00382-021-06018-x

Reale, O. & Atlas, R. (2001) Tropical cyclone–like vortices in the extratropics: observational evidence and synoptic analysis. *Weather and Forecasting*, 16(1), 7–34. Available from: https://doi.org/10.1175/JCLI-D-14-00339.1

Reed, R.J., Kuo, Y.-H., Albright, M.D., Gao, K., Guo, Y.-R. & Huang, W. (2001) Analysis and modeling of a tropical-like cyclonein the Mediterranean Sea. *Meteorology and Atmospheric Physics*, 76(1–4), 183–202. Available from: https://doi.org/10.1007/s007030170029

Renault, L., Chiggiato, J., Warner, J.C., Gomez, M., Vizoso, G. & Tintoré, J. (2012) Coupled atmosphere-ocean-wave simulations of a storm event over the Gulf of lion and Balearic Sea. *Journal of Geophysical Research: Oceans*, 117(C9), 2012JC007924. Available from: https://doi.org/10.1029/2012JC007924

Reynolds, R.W., Smith, T.M., Liu, C., Chelton, D.B., Casey, K.S. & Schlax, M.G. (2007) Daily high-resolution-blended analyses for sea surface temperature. *Journal of Climate*, 20(22), 5473–5496. Available from: https://doi.org/10.1175/2007JCLI1824.1

Ricchi, A., Miglietta, M., Barbariol, F., Benetazzo, A., Bergamasco, A., Bonaldo, D. et al. (2017) Sensitivity of a Mediterranean tropical-like cyclone to different model configurations and coupling strategies. *Atmosphere*, 8(5), 92. Available from: https://doi.org/10.3390/atmos8050092

Ricchi, A., Miglietta, M.M., Bonaldo, D., Cioni, G., Rizza, U. & Carniel, S. (2019) Multi-physics ensemble versus Atmosphere–Ocean coupled model simulations for a tropical-like cyclone in the Mediterranean Sea. *Atmosphere*, 10(4), 202. Available from: https://doi.org/10.3390/atmos10040202

Rizza, U., Canepa, E., Miglietta, M.M., Passerini, G., Morichetti, M., Mancinelli, E. et al. (2021) Evaluation of drag coefficients under medicane conditions: coupling waves, sea spray and surface friction. *Atmospheric Research*, 247, 105207. Available from: https://doi.org/10.1016/j.atmosres.2020.105207

Rizza, U., Canepa, E., Ricchi, A., Bonaldo, D., Carniel, S., Morichetti, M. et al. (2018) Influence of wave state and sea spray on the roughness length: feedback on Medicanes. *Atmosphere*, 9(8), 301. Available from: https://doi.org/10.3390/atmos9080301

Romero, R. (2008) A method for quantifying the impacts and interactions of potential-vorticity anomalies in extratropical cyclones. *Quarterly Journal of the Royal Meteorological Society*, 134(631), 385–402. Available from: https://doi.org/10.1002/qj.219

Ruti, P.M., Somot, S., Giorgi, F., Dubois, C., Flaounas, E., Obermann, A. et al. (2016) Med-CORDEX initiative for Mediterranean climate studies. *Bulletin of the American Meteorological Society*, 97(7), 1187–1208. Available from: https://doi.org/10.1175/BAMS-D-14-00176.1

Sanchez-Gomez, E. & Somot, S. (2018) Impact of the internal variability on the cyclone tracks simulated by a regional climate model over the med-CORDEX domain. *Climate Dynamics*, 51(3), 1005–1021. Available from: https://doi.org/10.1007/s00382-016-3394-y

Sanna, A., Lionello, P. & Gualdi, S. (2013) Coupled atmosphere ocean climate model simulations in the Mediterranean region: effect of a high-resolution marine model on cyclones and precipitation. *Natural Hazards and Earth System Sciences*, 13(6), 1567–1577. Available from: https://doi.org/10.5194/nhess-13-1567-2013

Sartini, L., Mentaschi, L. & Besio, G. (2015) Comparing different extreme wave analysis models for wave climate assessment along the Italian coast. *Coastal Engineering*, 100, 37–47. Available from: https://doi.org/10.1016/j.coastaleng.2015.03.006

Sauvage, C., Lebeaupin Brossier, C., Bouin, M.-N. & Ducrocq, V. (2020) Characterization of the air–sea exchange mechanisms during a Mediterranean heavy precipitation event using realistic sea state modelling. *Atmospheric Chemistry and Physics*, 20(3), 1675–1699. Available from: https://doi.org/10.5194/acp-20-1675-2020

Shchepetkin, A.F. & McWilliams, J.C. (2005) The regional oceanic modeling system (ROMS): a split-explicit, free-surface, topography-following-coordinate oceanic model. *Ocean Modelling*, 9(4), 347–404. Available from: https://doi.org/10.1016/j.ocemod.2004.08.002

Sikirić, M.D., Janeković, I. & Kuzmić, M. (2009) A new approach to bathymetry smoothing in sigma-coordinate ocean models. *Ocean Modelling*, 29(2), 128–136. Available from: https://doi.org/10.1016/j.ocemod.2009.03.009

Skamarock, W.C., Klemp, J.B., Dudhia, J., Gill, D.O., Barker, D.M., Duda, M.G. et al. (2008) A Description of the Advanced Research WRF Version 3 (No. NCAR/TN-475+STR). University Corporation for Atmospheric Research.

Skliris, N., Sofianos, S., Gkanasos, A., Mantziafou, A., Vervatis, V., Axaopoulos, P. et al. (2012) Decadal scale variability of sea surface temperature in the Mediterranean Sea in relation to atmospheric variability. *Ocean Dynamics*, 62(1), 13–30. Available from: https://doi.org/10.1007/s10236-011-0493-5

Somot, S., Ruti, P., Ahrens, B., Coppola, E., Jordà, G., Sannino, G. et al. (2018) Editorial for the med-CORDEX special issue. *Climate Dynamics*, 51(3), 771–777. Available from: https://doi.org/10.1007/s00382-018-4325-x

Soto-Navarro, J., Jordá, G., Amores, A., Cabos, W., Somot, S., Sevault, F. et al. (2020) Evolution of Mediterranean Sea water properties under climate change scenarios in the med-CORDEX ensemble. *Climate Dynamics*, 54(3–4), 2135–2165. Available from: https://doi.org/10.1007/s00382-019-05105-4

Stanev, E.V., Le Traon, P.-Y. & Peneva, E.L. (2000) Sea level variations and their dependency on meteorological and hydrological forcing: analysis of altimeter and surface data for the Black Sea. *Journal of Geophysical Research*, 76(24), 5877–5892.

Theurich, G., DeLuca, C., Campbell, T., Liu, F., Saint, K., Vertenstein, M. et al. (2016) The earth system prediction suite: toward a coordinated U.S. modeling capability. *Bulletin of the American Meteorological Society*, 97(7), 1229–1247. Available from: https://doi.org/10.1175/BAMS-D-14-00164.1

Thompson, P., Cai, Y., Reeve, D. & Stander, J. (2009) Automated threshold selection methods for extreme wave analysis. *Coastal Engineering*, 56(10), 1013–1021. Available from: https://doi.org/10.1016/j.coastaleng.2009.06.003

Tous, M. & Romero, R. (2013) Meteorological environments associated with medicane development. *International Journal of Climatology*, 33(1), 1–14. Available from: https://doi.org/10.1002/joc.3428

Tous, M. & Romero, R. (2011) Medicanes: cataloguing criteria and exploration of meteorological environments. *Tethys: Journal of*

Mediterranean Meteorology & Climatology, 8. Available from: https://doi.org/10.3369/tethys.2011.8.06

Turuncoglu, U.U. (2019) Toward modular in situ visualization in earth system models: the regional modeling system RegESM 1.1. *Geoscientific Model Development*, 12(1), 233–259. Available from: https://doi.org/10.5194/gmd-12-233-2019

Turuncoglu, U.U. & Sannino, G. (2017) Validation of newly designed regional earth system model (RegESM) for Mediterranean Basin. *Climate Dynamics*, 48(9–10), 2919–2947. Available from: https://doi.org/10.1007/s00382-016-3241-1

Varlas, G., Vervatis, V., Spyrou, C., Papadopoulou, E., Papadopoulos, A. & Katsafados, P. (2020) Investigating the impact of atmosphere–wave–ocean interactions on a Mediterranean tropical-like cyclone. *Ocean Modelling*, 153, 101675. Available from: https://doi.org/10.1016/j.ocemod.2020.101675

Warner, J.C., Perlin, N. & Skyllingstad, E.D. (2008) Using the model coupling toolkit to couple earth system models. *Environmental Modelling & Software*, 23(10–11), 1240–1249. Available from: https://doi.org/10.1016/j.envsoft.2008.03.002

Wiese, A., Staneva, J., Schulz-Stellenfleth, J., Behrens, A., Fenoglio-Marc, L. & Bidlot, J.-R. (2018) Synergy of wind wave model simulations and satellite observations during extreme events. *Ocean Science*, 14(6), 1503–1521. Available from: https://doi.org/10.5194/os-14-1503-2018

Zeng, X., Zhao, M. & Dickinson, R.E. (1998) Intercomparison of bulk aerodynamic algorithms for the computation of sea surface fluxes using TOGA COARE and TAO data. *Journal of Climate*, 11(10), 2628–2644. Available from: https://doi.org/10.1175/1520-0442(1998)011<2628:IOBAAF>2.0.CO;2

Zhao, W. & Chen, S.S. (2005) A Coupled Atmosphere-Wave-Ocean Framework for High-Resolution Modeling of Tropical Cyclones and Coastal Storms.

SUPPORTING INFORMATION

Additional supporting information can be found online in the Supporting Information section at the end of this article.

How to cite this article: Batibeniz, F., Önol, B., Turuncoglu, U.U. & Raible, C.C. (2025) Air–sea interaction in medicanes with atmosphere–ocean–wave coupled regional climate simulations. *Quarterly Journal of the Royal Meteorological Society*, e5040. Available from: https://doi.org/10.1002/qj.5040